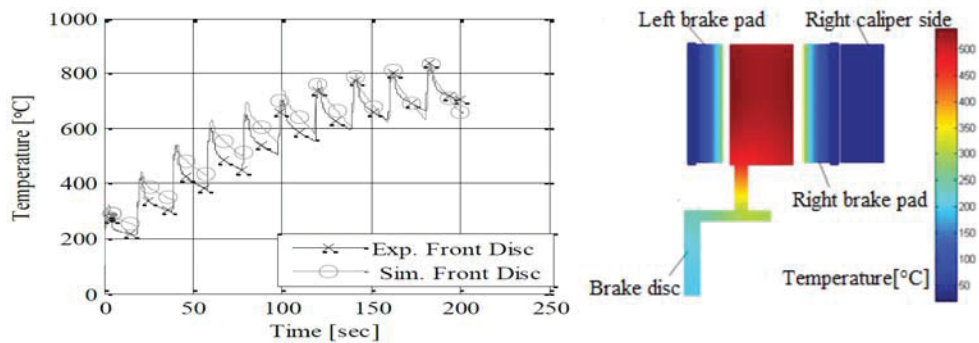


Heat Transient Transfer Analysis of Brake Disc/Pad System



Naga Vamsi Krishna Kora
Srivatsan Thuppal Vedanta

Department of Mechanical Engineering
Blekinge Institute of Technology
Karlskrona, Sweden

2016

HEAT TRANSIENT TRANSFER ANALYSIS OF BRAKE DISC /PAD SYSTEM

NAGA VAMSI KRISHNA KORA
SRIVATSAN THUPPAL VEDANTA

Department of Mechanical Engineering
Blekinge Institute of Technology
Karlskrona, Sweden,
2016

Thesis submitted for completion of Master of Science in Mechanical Engineering with emphasis on Structural Mechanics at Department of Mechanical Engineering, Blekinge Institute of Technology, Karlskrona, Sweden.

Abstract

Braking is mainly controlled by the engine. Friction between a pair of pads and a rotating disc converts the kinetic energy of the vehicle into heat. High temperatures can be reached in the system which can be detrimental for both, components and passenger safety. Numerical techniques help simulate load cases and compute the temperatures field in brake disc and brake pads. The present work implements a Finite Element (FE) toolbox in Matlab/Simulink able to simulate different braking manoeuvres used for brake dimensioning mainly in the early phase of car development process. The brake pad/disc geometry is considered as an axisymmetric body assuming negligible temperature gradient along the circumference of the disc. Calibration using three control factors namely: heat coefficient during braking (h_b), acceleration (h_a) and emissivity (ϵ) for the implemented thermal model is performed using experimental investigation at Volvo Car Corporation (VCC) for three specific severe load cases. The thermal model is extended to measure brake fluid temperatures to ensure no vaporisation occurs. Simulation results of the brake disc and brake pad show good correlation with the experimental tests. A sensitivity analysis with the control factors showed convective coefficient during acceleration h_a the most sensitive, with temperature change of around 16%.

Keywords: Brake disc, Brake dimensioning, Heat transient analysis, Finite Element, Calibration

ACKNOWLEDGEMENTS

This thesis work was carried out at Volvo Car Corporation (VCC), Gothenburg, Sweden in collaboration with the Department of Mechanical Engineering, Blekinge Institute of Technology (BTH), under the supervision of Dr. Ansel Berghuvud (BTH), Dr. Gael Le Gigan (VCC), Mr. Masoud Vahedi (VCC) and Dr. Sara Caprioli (VCC). Working with the brake performance team at Volvo was filled with learning experiences that helped us grow both on the personal and professional front.

We would like to show sincere gratitude towards our supervisors Gaël Le Gigan, Masoud Vahedi and Sara Caprioli for their relentless guidance and time throughout the process of learning, without whom the project would not have been possible. We would also like to thank our project managers Mikael Kjellgren and Mats Gustafsson for their administrative support while providing a wonderful work atmosphere.

We would endow credit to Blekinge University and our course educators Dr. Ansel Berghuvud and Dr. Johan Wall for their academic teachings, valuable inputs and tremendous support during this thesis.

Finally, we would like to express our love towards family members and friends for their eternal advice and encouragement.

Gothenburg, September 2016

Kora Naga Vamsi Krishna

Srivatsan Thuppal Vedanta

CONTENTS

Notations	4
List of Figures	6
List of Tables	9
Abbreviations	10
Definitions	11
1 Introduction	12
1.1 Aim and Objectives	15
1.2 Research Questions	16
2 Modelling	18
2.1 Finite element formulation of pad/disc system	18
2.2 Numerical brake disc model implementation in Matlab	23
2.3 Specific Assumptions and Boundary Conditions considered for modelling	28
2.4 Heat flow in brake disc system	30
2.5 Simulink Implementation	37
3 Calibration and Verification	39
3.1 Commercial Software	39
3.2 Measurement	44
3.3 Sensitivity analysis	52
4 Discussion and Conclusion	55
5 Future Work	60
6 References	62
7 Appendix	64

NOTATIONS

φ	Angle subtended by the pad at the centre of friction surface	radians
T_{∞}	Ambient temperature	°C/K
α_{pad}	Amount of radiation heat absorbed by the pad from the disc	-
ω	Angular velocity of the wheel	rad.s ⁻¹
A_{caliper}	Area of caliper	m ²
A_{disc}	Area of disc	m ²
A_{friction}	Area of friction surface	m ²
A_{pad}	Area of pad	m ²
F	Boundary load vector	-
P	Brake power	W
T_b	Brake torque	N-m
[C]	Capacity matrix	-
k	Conductivity	Wm ⁻¹ K ⁻¹
μ	Coefficient of friction	-
h	Convection heat coefficient	Wm ⁻² K ⁻¹
ρ	Density	kg.m ⁻³
ε	Emissivity	-
r_{eff}	Effective radius of the brake disc	m
Q	Heat flux	W.m ⁻²
f	Heat source	W
σ_{disc}	Heat partition to the disc	-
σ_{pad}	Heat partition to the pad	-
r_2	Inner radius of the friction surface	m

L	Internal energy	
<i>n</i>	Normal vector	-
<i>b</i>	Number of Iterations	
r_3	Outer radius of the friction surface	m
<i>p</i>	Pressure on the brake pedal	N.m ⁻²
ϕ	Shape function	-
<i>c</i>	Specific heat	Jkg ⁻¹ K ⁻¹
σ	Stefan Boltzmann constant	-
[K]	Stiffness matrix	-
<i>T</i>	Temperature	°C/K
<i>t</i>	Time	s
λ	Tolerance limit	
k_w	Wear coefficient	

LIST OF FIGURES

<i>Figure 1.1. Band brake (left) and drum brake (right).</i>	12
<i>Figure 1.2. Different vane types of brake discs (from front to back: curved vane, radial vanes and pillars).</i>	13
<i>Figure 1.3. “Exploded” view of brake caliper assembly.</i>	14
<i>Figure 1.4. Detailed view of brake system.</i>	14
<i>Figure 1.5. Coordinated Problem Approach.</i>	15
<i>Figure 2.1. Ventilated (left) and solid (right) brake discs.</i>	25
<i>Figure 2.2. Illustration of two independent sections with different mesh sizes. Note that the right figure has the two sections separated for better clarity whereas it defines the same body.</i>	26
<i>Figure 2.3. Two meshed sections with identical mesh sizes. The sections display two different node numbers at the contact interface as shown by the circled regions.</i>	27
<i>Figure 2.4. Division of the sections to fulfil criteria of compatible node numbers at the boundaries (left) and fulfilment of compatibility at the interaction boundary (right).</i>	27
<i>Figure 2.5. Heat input and dissipation from the brake disc and brake pads during heating phase (left) and cooling phase (right).</i>	29
<i>Figure 2.6. Uniform pressure model in brake disc (left) and brake pad (right).</i>	31
<i>Figure 2.7. Uniform wear model in brake disc (left) and brake pad (right).</i>	31
<i>Figure 2.8. Brake power distribution flowchart.</i>	33
<i>Figure 2.9. Contact surface element in disc (left) and pad (right).</i>	34
<i>Figure 2.10. Block diagram of brake disc thermal model in Simulink</i>	37
<i>Figure 3.1. Axisymmetric rectangular block undergoing heat dissipation via three modes of heat transfer.</i>	40
<i>Figure 3.2. Transient heat model undergoing convection and radiation heat transfer on an axisymmetric rectangle from both MATLAB (above) and ABAQUS (below). Note the temperatures mentioned in the axis are in Kelvin scale.</i>	40
<i>Figure 3.3. Indicates brake disc with the regions of imposed heat flux boundary.</i>	41
<i>Figure 3.4. Transient analysis with convection and radiation during heating phase at time $t=5$ s in Abaqus (above) and Matlab (below). Note that the temperatures mentioned in the axis are in Kelvin.</i>	42

Figure 3.5. Transient analysis with convection and radiation during heating phase at time $t=10$ s in Abaqus (above) and Matlab (below). Note the temperatures mentioned in the axis are in Kelvin.	43
Figure 3.6. Nodal temperature difference between Matlab and Abaqus model at the end of the heating phase (left) and at the end of the cooling phase (right).	44
Figure 3.7. Position (marked by red circles) of thermocouples on the front (left) and rear (right) pads.	45
Figure 3.8. Position (marked by red circles) of thermocouples embedded at a distance of 2mm inside the front (left) and rear (right) disc.	45
Figure 3.9. Test Case I calibration (Sim) and experimental (Exp) temperature results for the front disc (left) and the front pad (right). Note the different temperature scales for the vertical axis.	47
Figure 3.10. Test Case I calibration (Sim) and experimental (Exp) temperature results for the rear disc (left) and the rear pad (right). Note the different scales on the vertical axis.	47
Figure 3.11. Test Case II calibration (Sim) and experimental (Exp) temperature results of the front disc (left) and the front pad (right). Note the different scales on the vertical axis.	48
Figure 3.12. Test Case II calibration (Sim) and experimental (Exp) temperature results of the rear disc (left) and the rear pad (right). Note the different scales on the vertical axis.	49
Figure 3.13. Test Case III calibration (Sim) and experimental (Exp) temperature results of front brake disc (left) and the front brake pad (right). Note the different scales on the vertical axis.	50
Figure 3.14. Test Case III calibration (Sim) and experimental (Exp) temperature results of the rear brake disc (left) and the rear brake pad (right). Note the different scales on the vertical axis.	51
Figure 3.15. Test Case III calibration (Sim) and experimental (Exp) temperature results of brake fluid at the front axle (left) and rear axle (right). Note the different scales on the vertical axis.	51
Figure 3.16. Sensitivity analysis correlation with convection coefficient while braking and accelerating with $h_a = 90$ and $h_b = 60$.	53
Figure 3.17. Sensitivity correlation compared with emissivity 0.6.	54
Figure 7.1. L-shaped cross-section	64
Figure 7.2. Element and node numbers defined for the cross-section	65
Figure 7.3. Matlab geometry definition.	65
Figure 7.4. Element and mesh configurations in Matlab.	66
Figure 7.5. Geometry with boundary compatibility between sections.	66

Figure 7.6. Mesh configuration of cross-section showing node numbers (left) and element numbers (right). _____ 67

LIST OF TABLES

<i>Table 2.1. Parameters for creating the brake disc and brake pad geometry.</i>	25
<i>Table 3.1. Parameters for transient analysis</i>	39
<i>Table 3.2. Temperature evolution table for the transient analysis.</i>	44
<i>Table 3.3. Parameters for the calibration of Test case I.</i>	46
<i>Table 3.4. Parameters for calibration of Test case II.</i>	48
<i>Table 3.5. Material properties of brake disc system.</i>	50
<i>Table 3.6. Parameters for calibration of Test case III.</i>	50
<i>Table 3.7. Percentage change in temperature for test Case I Test (a).</i>	52
<i>Table 3.8. Percentage change in temperature for test Case I Test (b).</i>	53
<i>Table 3.9. Percentage change in temperature for test Case 2.</i>	54

ABBREVIATIONS

CAE.....	Computer Aided Engineering
FE	Finite Element
FDM	Finite Difference Method
FEM.....	Finite Element Method
VCC.....	Volvo Car Corporation

DEFINITIONS

Brake caliperthe assembly housing the brake pads and pistons which help initiate braking action.

Brake discis the component of the disc brake system against which the pads act generating friction thereby retarding the vehicle.

Brake padis a part of the caliper assembly which produces friction on the brake disc surface and initiates braking.

CALFEMComputer Aided Learning of the Finite Element Method developed by Division of Structural Mechanics, Lund University.

1 Introduction

Over the years, car manufacturers are constantly seeking enhancement of vehicle dynamics and passenger comfort, simultaneously maintaining vehicle aesthetics and quality. A key component of the safety feature is the brake system, while there are other active and passive safety components to support the system in an attempt to mitigate injuries. The need for safe transportation has brought about developments with the brake system making it withstand and fulfil rigorous braking manoeuvres under various situations such as dry, humid, wet, cold or warm environment and traffic conditions.

Early invention of the brake system saw two variants namely “*band*” and “*drum*” brakes, both using the principle of mechanical linkage. Band brakes had a prolific use throughout the 18th century having a compact wooden block [1]. The brake application was fulfilled by pulling a lever at a hands distance, see Figure 1.1 (left). Drum brakes, see Figure 1.1 (right), were invented by Louis Renault in 1902 [1]. Inherent performance and robust design of drum brakes is the reason for their rapid use even today in the rear axle in some vehicles.

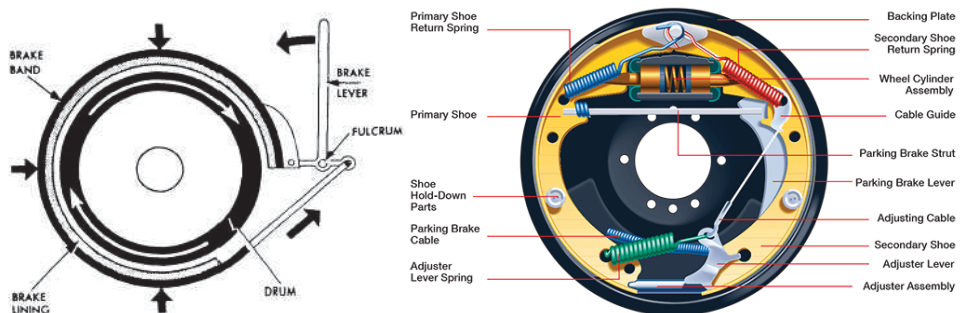


Figure 1.1. Band brake (left) and drum brake (right) [2], [3].

Subsequently, Malcolm Loughhead brought the concept of hydraulic powered brakes, also known as “*disc brakes*”, which found application in the latter half of 19th century [1]. Brake discs are capable of dissipating heat from its surfaces as the friction area and vents are open to air compared to drum brakes. When driven through water, brake discs are able to wipe off the water quickly. However a noted disadvantage of brake disc is that they are open to corrosion from water and wear. Brake discs are classified based on their surface as cross-drilled, slotted or flat. They are further classified based on

their design as solid or ventilated discs. The ventilated discs consist of straight, tangential vanes, curved vanes or pillars, see Figure 1.2.



Figure 1.2. Different vane types of brake discs (from front to back: curved vane, radial vanes and pillars) [4].

Background

Volvo Car Corporation (VCC), one of the leading car manufacturer, has been the face of safety innovations such as seatbelt and child seat. Volvo's vehicles are globally known for their reliability and safety engineering attributes. As competitors in the global market, Volvo has been able to produce a wide range of passenger cars for different customer needs. Also Volvo is successful in maintaining and improving standards creating a healthy atmosphere of support. Moreover, Volvo is highly involved in sustainability and autonomous driving which demands much higher advance active safety features compared to the traditional technologies.

Nowadays, CAE simulations are becoming more prominent to verify different design specifications in an attempt to decrease cost, development time and number of test vehicles. The process of finding the most optimum brake components combination for each vehicle specification is called brake dimensioning. The brake discs, brake pads and calipers at the front and rear of the vehicle are only few examples of those common components which should be decided on during the brake dimensioning process. The output of current thesis will be used in such phases at VCC as part of the brake dimensioning toolbox.

Brake System Description.

The brake system is composed of a brake pedal (main actuator), vacuum booster, modulation unit, a master cylinder, caliper assembly, see Figure 1.3, and brake disc.

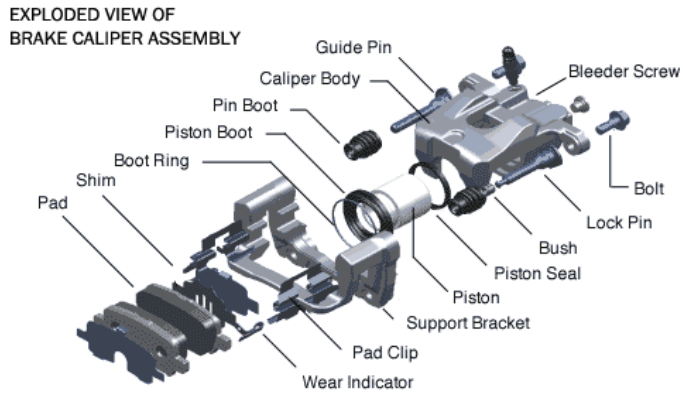


Figure 1.3. “Exploded” view of brake caliper assembly [5].

The force on the brake pedal determines the pressure generated in the master cylinder. A vacuum booster has been an addition to the brake system which helps generate about 10 times the force exerted on the brake pedal. The booster creates additional pressure to reduce excessive brake pedal thrust and movement. Further, the force on the brake pedal is distributed via the hydraulic unit shown in Figure 1.4 to actuate the calipers. Thus creating a frictional force on the disc in turn retarding the wheel. The hydraulic unit comprises of a master cylinder which contains two inlet ports, compensation ports and a couple of piston rods to transfer the fluid from the reservoir into the caliper assembly. The piston transfers the fluid from the master cylinder to enable braking through brake pads which are a part of the caliper assembly. Generally, fixed and floating are the two caliper types used.

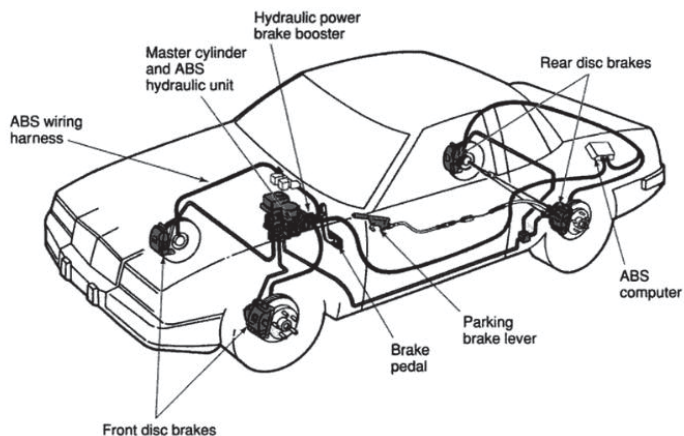


Figure 1.4. Detailed view of brake system [6].

1.1 Aim and Objectives

The aim of the present work is to implement a thermal model which calculates brake disc and brake pad temperatures for brake dimensioning in the early stages of car development process. The simulation results from the thermal model are calibrated against three test cases with the experimental test data obtained from VCC. The FE tool is implemented in Matlab while the braking manoeuvres are tested in Simulink. The present work is based on the coordinated approach shown in Figure 1.5.

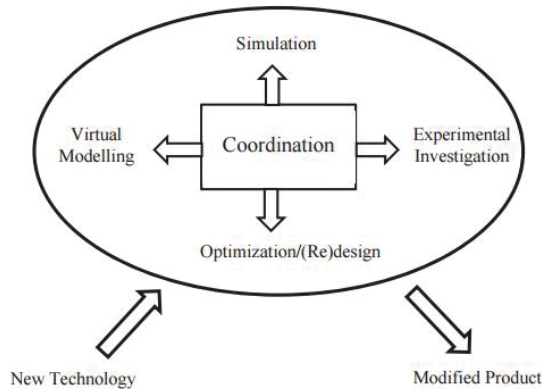


Figure 1.5. Coordinated Problem Approach [7].

The aim is met through the following guidelines:

1. Literature study of 1) brake system types and functioning and 2) thermal models to get an insight of transient heat transfer equations, heat distribution and temperature evolutions in brake disc and brake pads.
2. Verifying the CALFEM/Matlab FE code with a simple rectangular 2-D axisymmetric plate in Simulia/Abacus.
3. Extension of the model to the actual brake disc geometry by implementing appropriate boundary conditions.
4. Calibration of the model against experimental data for three different test cases.
5. Implement the thermal model in Simulink to integrate with car software for future simulations.

1.2 Research Questions

1. How do the braking manoeuvres influence brake disc and brake pad temperatures?
2. What is the impact of temperature and velocity on heat dissipation coefficients?
3. How to handle brake fluid temperatures in an axisymmetric model?

Literature study

Secrist D.A. and Hornbeck R.W. [8] analyse the heat transfer and fade (gradual decrease in the ability to stop due to continuous braking) in brake disc based on the following assumptions: 1) braking effort (brake torque) is shared equally between the each of the wheels in case of both, the front and rear axles and 2) the temperature of the disc varies only with radial position and time.

Talati F. and Jalalifar S. [9], states that modelling the thermal contact between the brake pad and brake disc has two approaches: 1) perfect thermal contact or 2) imperfect thermal contact. The imperfect thermal contact can be further modelled based on the case as uniform pressure or uniform wear.

Rao S.S.[10] and Broman G. [7] outline Fourier's heat equations and the finite element formulations for non-linear problems to obtain nodal temperatures. Kythe P.K. [11] examines axisymmetric FE equations for heat transfer problems with linear triangular elements which are implemented in the present work.

According to Yevtushenko A. A. and Grzes P. [12], heat partitioning coefficient is calculated from the disc and pad material properties for heat distribution in the disc brake system. The paper explains the influence of formulae for heat partition on temperatures for two different brake disc systems. The accuracy of temperature evolution will depend on the heat partition ratio formula. In addition, greater thickness of the brake pad and smaller heating depth have constant heat partition ratios. Heat partition coefficient is calculated according to the standard formulae stated in the literatures [9], [12].

The heat dissipation coefficients and the boundary conditions of the transient analysis are considered from Eisengräber R. et al. [13].

2 Modelling

CAE modelling approach, concepts related to heat transfer and the governing equations used in the thermal model are presented in the following. The brake disc and brake pad geometry and their respective material properties are provided by VCC. Generally, heat transfer problems can be modelled using two approaches: Finite Difference Method (FDM) or Finite Element Method (FEM). FDM is based on the application of Taylor series expansion to approximate Partial Differential Equations (PDE). It uses square line network topology to discretize elements. The method is simple for extending to a higher order accuracy though taking a lot of computational time. FEM on the other hand involves mapping a set of functions from vector space to real numbers. This method is suitable for complex geometries and domains involving discontinuities. Higher order accuracy is obtained with the help of shape functions. FEM is usually preferred over FDM because of its ease in incorporation of boundary conditions as well as its compatibility for complex geometries. FEM generates solutions by using piecewise defined functions which help interpolate smoothly over the domain without losing much accuracy [14]. Based on the above reasoning, thermal model for brake disc is implemented using FEM in the present work.

2.1 Finite element formulation of pad/disc system

The brake disc thermal model makes use of axisymmetric modelling. In an axisymmetric model, a two dimensional section, when revolved, yields to a three dimensional model. The temperature gradient in the circumferential direction is neglected for heat transfer problems in this model. The use of symmetry is beneficial to avoid repetitive boundary conditions. Also, the size of stiffness matrix *i.e.* number of elements can be reduced considerably leading to a decrease in cost and computational time [11].

Axisymmetric finite element equations for heat transfer from a body

The heat is dissipated through three heat transfer modes: conduction, convection and radiation which are explained as follows:

- Conduction is the heat transfer between adjoining regions of contact (while both materials are not in motion) through molecular agitation where heat is transferred directly through the material due to difference in temperatures or electric potential.

- Convection is defined as the heat transfer involving motion of a fluid against a solid when the heated fluid expands and moves away from the heat source either under the influence of buoyancy or forced by external agents. The former process is called as natural convection and the latter forced convection.
- Radiation is the transfer of energy by vacuum or through a solid or fluid medium by means of electromagnetic waves carrying thermal energy. The possible boundary conditions of all three modes of heat transfer (*i.e.* conduction, convection and radiation) are implemented in this work to identify the temperature evolution at the brake disc and brake pad surfaces respectively.

The transient heat conduction equation in a three dimensional solid having convection and gradient boundaries is based on Fourier's law as outlined in Kythe P.K. [11] which is expressed as

$$-k \left(\frac{\partial^2 T}{\partial x^2} + \frac{\partial^2 T}{\partial y^2} + \frac{\partial^2 T}{\partial z^2} \right) = f - \rho c \frac{\partial T}{\partial t} \quad (1)$$

where T [K] is the temperature, f [W] is the heat source, c [$\text{Jkg}^{-1}\text{K}^{-1}$] is the specific heat, ρ [kg.m^{-3}] is the density, t [s] is the time, $[\mathbf{x}, \mathbf{y}, \mathbf{z}]$ are the respective co-ordinate planes, k [$\text{Wm}^{-1}\text{K}^{-1}$] is the heat conductivity which is constant in all three planes.

$$T = \dot{T} \text{ on boundary } C1$$

where \dot{T} is the time dependent temperature derivative.

$$-k\nabla T \cdot \mathbf{n} = h(T - T_\infty) \text{ on boundary } C2$$

where ∇ is partial double differential operator, \mathbf{n} is the normal vector, h [$\text{Wm}^{-2}\text{K}^{-1}$] is the convection heat coefficient, T_∞ [K] is the ambient temperature.

The steps followed in FE formulation and solution of a problem are [7]

- Transform the strong form in equation (1) into the weak form.
- Choose trial functions, *i.e.* element type(s), and mesh the solution domain.
- Multiply the differential equation with a weight function and establish a system of algebraic equation for each element.

- Assemble these element equations into a global algebraic system of equations.
- Incorporate boundary conditions into the global system of equations.
- Solve the global system of equations for the unknowns and interpret the results.

The variables $f, \dot{T}, k, \beta, T_\infty$ in equation (1) are assumed to be functions of polar coordinates (r, z) to imply an axisymmetric case. Following the steps described above, the three dimensional transient heat equation according to Kythe P.K. [11] is solved for the weak form as

$$\begin{aligned}
& \int k \nabla T \cdot \mathbf{n} \cdot \varnothing^{(e)} r ds + \int h T_\infty \cdot \varnothing^{(e)} r ds + \iint \varnothing^{(e)} f r dr dz \\
& = \left[\iint k \left(\frac{\partial \varnothing^{(e)}}{\partial r} \frac{\partial (\varnothing^{(e)})'}{\partial r} \right. \right. \\
& \quad \left. \left. + \frac{\partial \varnothing^{(e)}}{\partial z} \frac{\partial (\varnothing^{(e)})'}{\partial z} \right) r dr dz \right] T^{(e)} \\
& + \left[\int h \varnothing^{(e)} (\varnothing^{(e)})' r ds \right] T^{(e)} \\
& + \left[\int \rho c \varnothing^{(e)} (\varnothing^{(e)})' r ds \right] \dot{T}^{(e)}
\end{aligned} \tag{2}$$

where $\varnothing [-]$ is the shape function, $(\blacksquare)'$ represents transpose of the equation, $(\blacksquare)^{(e)}$ represents element form.

Equation (2) can be reformulated as

$$\mathbf{C}^{(e)} \dot{T}^{(e)} + \mathbf{K}^{(e)} T^{(e)} = \mathbf{F}^{(e)} + \mathbf{L}^{(e)} \tag{3}$$

where Stiffness matrix $\mathbf{K} = \iint k \left(\frac{\partial \varnothing^{(e)}}{\partial r} \frac{\partial (\varnothing^{(e)})'}{\partial r} + \frac{\partial \varnothing^{(e)}}{\partial z} \frac{\partial (\varnothing^{(e)})'}{\partial z} \right) r dr dz + \int h \varnothing^{(e)} (\varnothing^{(e)})' r ds$

Capacity matrix $\mathbf{C} = \int \rho c \varnothing^{(e)} (\varnothing^{(e)})' r ds$

Boundary load for convection $\mathbf{F}_c = \int h T_\infty \varnothing^{(e)} r ds + \iint \varnothing^{(e)} f r dr dz$

Internal energy $\mathbf{L} = \int k \nabla T \cdot \mathbf{n} \varnothing^{(e)} r ds$

Heat transfer equation in a body involving radiation

The general mathematical expression for heat transfer influenced by radiation is given as

$$Q_{radiation} = \sigma \varepsilon A (T^4 - T_{\infty}^4) \quad (4)$$

where σ [-] Boltzmann constant, ε [-] is the emissivity of the surface, A is the surface area in m^2 .

The radiation heat transfer can be transformed from equation (4) into [10]

$$Q_{radiation} = \sigma \varepsilon (T^2 + T_{\infty}^2)(T + T_{\infty}) \quad (5)$$

For radiation, stiffness and boundary load terms $\mathbf{K}_r^{(e)}$ and $\mathbf{F}_r^{(e)}$ are added to equation (2) whose values are given as

$$[\mathbf{K}_r^{(e)}] = \iint h(\vartheta^{(e)})^T \vartheta^{(e)} ds \quad (6)$$

$$\mathbf{F}_r^{(e)} = \iint h T_{\infty} (\vartheta^{(e)})^T ds \quad (7)$$

Equation (3) of heat transfer including radiation, is then expressed as

$$\mathbf{C}^{(e)} \dot{T}^{(e)} + (\mathbf{K}^{(e)} + \mathbf{K}_r^{(e)}) T^{(e)} = \mathbf{F}_c^{(e)} + \mathbf{L}^{(e)} + \mathbf{F}_r^{(e)} \quad (8)$$

The iterative procedure for the initial temperature will then be incorporated by the following

1. Consider the iteration number n as 1, assuming the value for $h^{(e)}$,
2. With the help of updated $h^{(e)}$ value, generate $\mathbf{K}_r^{(e)}$ and $\mathbf{F}_r^{(e)}$, see equations (6) and (7),
3. The element matrices and vectors are assembled to obtain the overall equation (8). Equation (9) and (10) show the assembled $[\mathbf{K}]$ and $\mathbf{F}^{(e)}$ matrices.

$$[\mathbf{K}] = \sum_{e=1}^E ([\mathbf{K}^{(e)}] + [\mathbf{K}_r^{(e)}]) \quad (9)$$

$$\mathbf{F}^{(e)} = \sum_{e=1}^E ([\mathbf{F}_c^{(e)}] + [\mathbf{F}_r^{(e)}]) \quad (10)$$

4. Solve equation (11) to obtain T ,

$$[\mathbf{C}]^{(e)} \dot{T}^{(e)} + [\mathbf{K}]^{(e)} T^{(e)} = \mathbf{F}^{(e)} \quad (11)$$

5. From the obtained nodal temperatures T , deduce new $h^{(e)}$ values. The average of the nodal two temperatures of the element, $(T_i + T_j)/2$ can be used as $T_{av}^{(e)}$ instead of T as in equation (12).

$$h^{(e)} = \sigma \varepsilon \left(T_{av}^{(e)2} + T_{\infty}^2 \right) \left(T_{av}^{(e)} + T_{\infty} \right) \quad (12)$$

If $n > 1$, test for convergence is given by equation (13) and (14),

$$\left| \frac{|h^{(e)}|_b - |h^{(e)}|_{b-1}}{|h^{(e)}|_{b-1}} \right| \leq \lambda_1 \quad (13)$$

and

$$\left| |(T^{total})_b - (T^{total})_{b-1}| \right| \leq \lambda_2 \quad (14)$$

where λ_1 and λ_2 are the tolerance limits. If the method is said to be converged, then stop the iteration by considering $\hat{T}(correct) = \hat{T}_b$, if it doesn't satisfy the condition then change the iteration number to $b = b + 1$ and continue the procedure from step 2.

2.2 Numerical brake disc model implementation in Matlab

The brake disc and brake pad system are modelled by the FE method using CALFEM (Computer Aided Learning of the Finite Element Method) functions in Matlab developed at Lund University during the late 1970's. Its application is for pure solid structures, heat transfer problems and modal analysis. CALFEM is used for its versatility, problem handling and the ease of understanding FEM [15]. In this thesis, a combination of default and modified CALFEM functions are used to generate the mesh over the brake disc and brake pad system (see Appendix).

The model considers a rectangular cross-section for the brake disc and brake pad geometries. Using the geometrical parameters shown in Table 2.1, the vertices, line segments and surfaces are defined to obtain the brake disc and brake pad geometry displayed in Figure 2.1.

Initially, all cross-sections are constructed from the parameters in Table 2.1 given as an input to Matlab. Finally, the brake disc geometry is divided into sub-sections to fulfil the mesh compatibility across the boundaries. The mesh compatibility criteria in the brake disc model is explained in detail by illustrations. For instance, the section 1 (bottom) and section 2 (top) in Figure 2.2 had to be divided because of incompatibility between nodes at the contact interface.

Figure 2.2 (right) illustration is for a better understanding whereas in reality the two sections are in contact i.e. the distance between them (say d) is zero. The two independently meshed sections with different sizes (length and width) produce different node numbers at the contact interface. For the heat to propagate between the two sections with a different mesh size, the intermediate nodal values should be defined as a function of the adjacent nodal values for the two sections, *i.e.* node 52 should be defined in Matlab as a function of adjacent nodes 44 and 60 as $T(52) = a \times T(44) + b \times T(60)$ and nodal value 44 must be equal to the value at node 25. To avoid this complexity in defining the heat distribution between the two sections for numerical solving they are chosen to have an identical mesh size.

As shown in Figure 2.3, even though the sections have the same mesh size, the domain mesh using CALFEM produces two different node numbers at

the same contact interface. Thus, the geometry was divided using intermediate sections as seen in Figure 2.4. The mesh for the brake disc and pads geometry is generated using linear triangular elements using a mesh density of 1mm across the domain of the brake disc.

The reasons for discretizing the brake disc geometry into 1mm fine element mesh are listed below:

- To maintain ideal aspect ratio, *i.e.* 1. A larger aspect ratio will have the effect of an interpolation error [16].
- For having mesh compatibility between adjacent components for example, brake disc and brake pads (as explained in the above figures). The possible mesh sizes which could be used are of the order $\frac{1}{q}$, where $q = 1,2,3 \dots$

However, the pad has a mesh size of 0.5 mm to obtain the required propagation of heat within the pad by having a finer mesh. The CPU time for the analysis would increase as the mesh size decreases. Hence to strike a balance between CPU time and a good mesh, the element size was considered as 1mm for the brake disc and 0.5 mm for the brake pad.

Use of triangular mesh is more suited for applications involving unstructured grids (complex geometries comprising curved surfaces, discontinuities) in comparison to a quadrilateral mesh. Importing the unstructured mesh geometries having a triangular mesh into Matlab from FE solvers such as Simulia/Abaqus, ANSA, etc. produces a well-defined calculation domain [16].

Table 2.1. Parameters for creating the brake disc and brake pad geometry.

Disc outer radius	R_0
Friction surface radial width (inner-outer)	R_d
Hub outer radius	Rh_0
Hub inner radius	Rh_i
Driveshaft hole radius	R_a
Disc1 thickness (if vent.)	Zd_1
Disc2 thickness connected to hat	Zd_2
Hub total axial length	Z_h
Dist. from hub outer surf. to disc	Z_d
Dist. from hub outer surf. to neck	Z_n
Dist. from hub inner edge to neck	Z_f
Hub outer surface thickness	Z_a
Ventilation section axial width	Z_v
Pad thickness	P_t
Pad height	P_h
Effective radius	R_{eff}

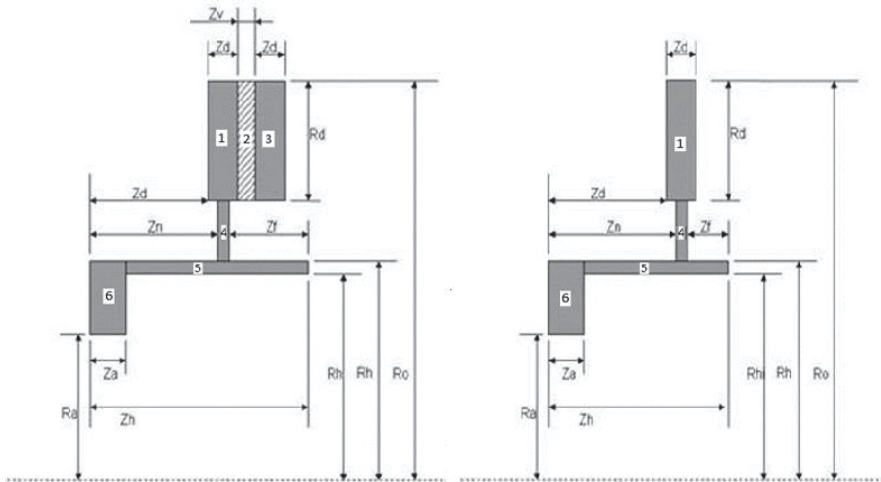


Figure 2.1. Ventilated (left) and solid (right) brake discs.

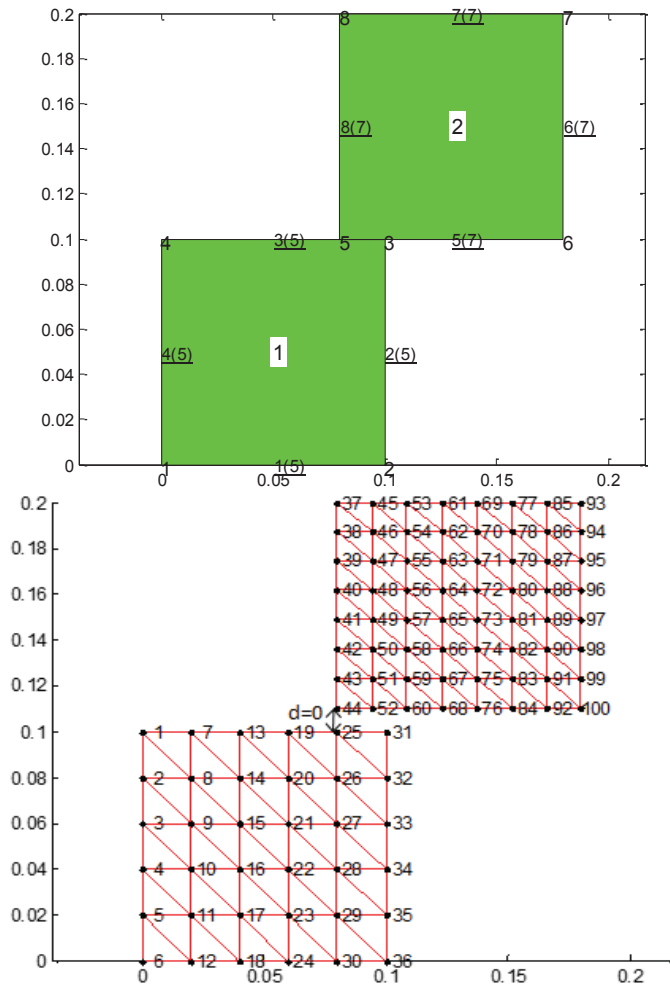


Figure 2.2. Illustration of two independent sections with different mesh sizes. Note that the right figure has the two sections separated for better clarity whereas it defines the same body.

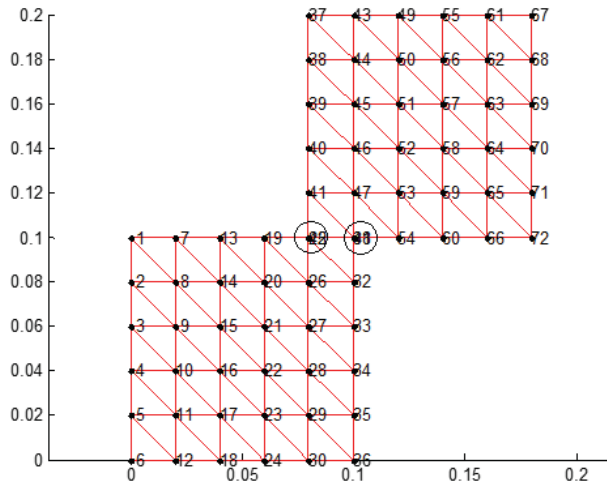


Figure 2.3. Two meshed sections with identical mesh sizes. The sections display two different node numbers at the contact interface as shown by the circled regions.

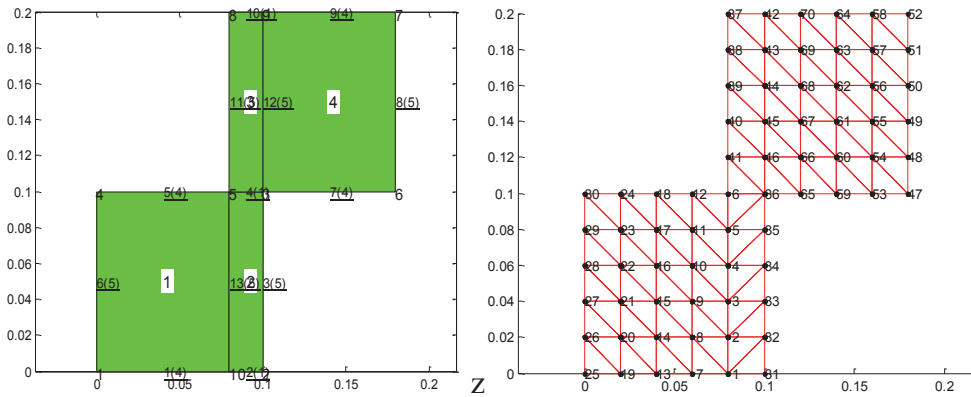


Figure 2.4. Division of the sections to fulfil criteria of compatible node numbers at the boundaries (left) and fulfilment of compatibility at the interaction boundary (right).

Further in the model, convection and radiation boundaries are prescribed to the corresponding line segment numbers. The convection and radiation heats are calculated at each time step for every element in the domain and the element matrices are finally assembled into global stiffness $[\mathbf{K}]$, capacity $[\mathbf{C}]$ and boundary load $[\mathbf{F}]$ matrices respectively.

The temperature at the brake disc and brake pad is then calculated with the formula specified below [7]:

$$\{\tilde{T}\}_{b+1} = [[\mathbf{C}] + \theta \cdot \Delta t[\mathbf{K}]]^{-1} [[\mathbf{C}] - (1 - \theta) \cdot \Delta t[\mathbf{K}]] \cdot \{\tilde{T}\}_b \quad (15)$$

where Δt is time increment,

$\theta = 0$, for forward difference Euler,

$\theta = 0.5$, Trapezoidal rule; Crank-Nicholson,

$\theta = 1$, for backward difference Euler.

According to Broman [7], for $\theta = 0$ (forward difference approximation) and $\theta = 1$ (backward difference approximation) the truncation error is of the first order. While the error is of second order if and only if $\theta = 0.5$, *i.e.* Crank Nicholson method. Also, the marching procedure of the solution is unconditionally stable for $\theta \geq 0.5$. Thus having $\theta = 0.5$ provides accuracy and stability to the solution [7]. The temperature iteration given by equation (15) continues until the difference between temperatures reaches below the set tolerance limit.

2.3 Specific Assumptions and Boundary Conditions considered for modelling

The brake disc and brake pads are modelled based on the following assumptions:

- The thermal model of brake disc is axisymmetric. The conductivity of the brake pad is scaled according to $\frac{\varphi}{2\pi}$, *i.e.* the ratio of frictional surface to pad area, (where φ is the angle subtended by the pad at the centre of the friction surface) as they cover only a sector of the friction surface.
- Vanes are modelled as a solid because they are complex to implement in an axisymmetric model. However, convection and radiation boundaries are given to the brake disc surface to have the behaviour

of the ventilated vanes. In addition, a part of brake disc section has a specific heat c of $50 \text{ [Jkg}^{-1}\text{K}^{-1}\text{]}$.

- The heat flux on the hat side and piston side in the brake disc is distributed equally. The phenomenon of brake disc coning is neglected, when the temperature on the hat side is around 10% higher than that of the piston side.
- Constant values of convection heat transfer coefficient h and emissivity ε are considered at the boundaries. Those values are tweaked in order to calibrate the brake disc temperatures against the experimental tests (see section 3).
- Radiation from the disc during cooling phase is considered to dissipate homogenously to the pads.
- Caliper and shims are together modelled as a simple axisymmetric rectangular block.

The convection and radiation boundaries in the brake disc, brake pads and caliper are shown in Figure 2.5. Convection heat transfer is most important in case of cooling while radiation is prominent as the temperatures are higher.

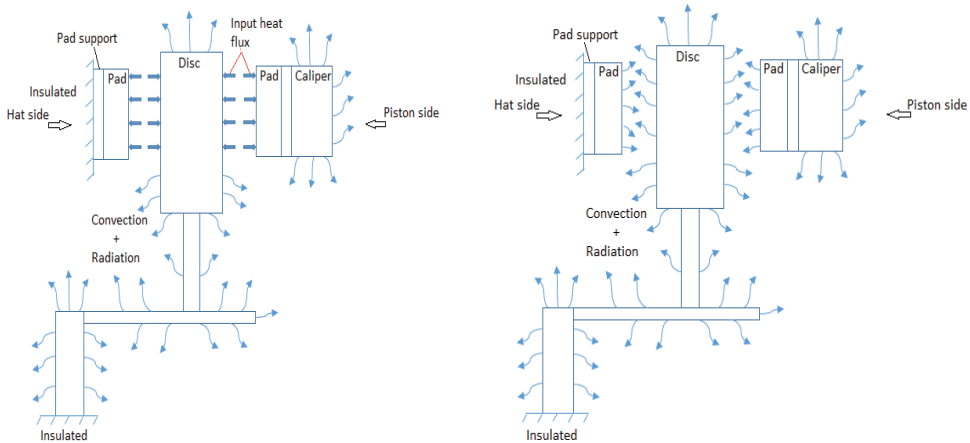


Figure 2.5. Heat input and dissipation from the brake disc and brake pads during heating phase (left) and cooling phase (right).

2.4 Heat flow in brake disc system

Disc/pad heat distribution.

In the following, friction modelling of the brake disc and brake pad contact interface is explained. The friction contact model has two approaches: uniform pressure and uniform wear given by Talati F. and Jalalifar S. [9].

Uniform pressure

Uniform pressure is displayed in Figure 2.6, having $p = p_{\max} = \gamma$, where γ is a constant and p_{\max} is the maximum pressure in pad-disc interface. For a new pair of brake pads, the uniform pressure model is valid. A constant pressure model has heat flux increasing in the radial direction [5].

Uniform wear

Uniform wear distribution is defined as $\delta = k_w p r = \text{constant}$, yielding $p = p_{\max} \times \frac{r_2}{r}$ where δ represents wear, k_w is wear coefficient, r_2 is inner radius of the pad and p is the pressure at radial position r .

For the case of uniform wear, see Figure 2.7, there are two consequences associated with the braking action [5] First, during the sliding contact the relative velocity increases with increase in radial direction. This velocity difference generates a higher temperature at the outer radius than at the inner radius. Second, there is a temperature gradient along the longitudinal direction of the pad. Apart from the area which is in contact with the disc surface, the remaining part of the brake disc gets time to cool before it comes into contact with the leading edge (the edge where disc initially comes in contact) of the pad. Thus, creating a temperature gradient between the leading edge and trailing edge of the pad [5].

In addition, the pad begins to wear due to repeated frictional force. This induced wear reduces the contact area of the pad thereby reducing the contact pressure. Reduced contact pressures lead to less heat generation considering a constant heat distribution over the pad surface. Hence over a period of time, the constant wear model is valid [5].

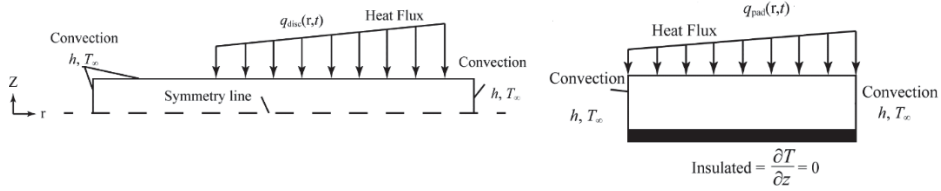


Figure 2.6. Uniform pressure model in brake disc (left) and brake pad (right) [9].

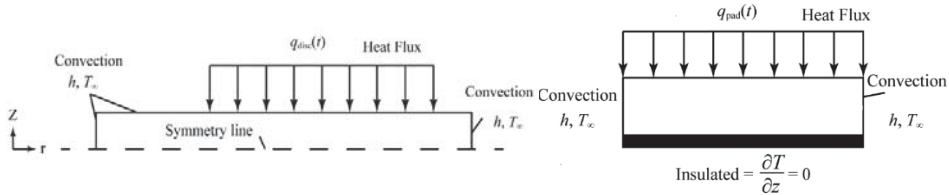


Figure 2.7. Uniform wear model in brake disc (left) and brake pad (right) [9].

Uniform pressure and uniform wear can be further modelled as perfect thermal contact or imperfect thermal contact. Perfect thermal contact at the brake disc and brake pad interface assumes identical surface temperatures on both the brake pad and brake disc, at the time of their contact. In reality, existence of perfect thermal contact is not possible because of the pad wear and thermal expansion due to repeated use. Imperfect thermal contact on the other hand assumes a temperature gradient between the pad and disc interface [9]. Hence the assumption of imperfect contact is used in the current work.

The imperfect thermal contact assumption can be modelled as a third body layer between the pad and disc as described in Talati F. and Jalalifar S. [9]. The so called third body layer is formed from plastic deformation, wear particles and chemical reaction which affects the friction behaviour between the pad and disc [9]. It is introduced to account for the friction behaviour at the time of contact between the brake disc and brake pad. In this work, an attempt to include a third body layer in the brake disc and brake pad model was made. However, due to difficulty in the estimation of heat distribution between disc and pad in presence of the third body, the idea was not carried forward. Hence, heat distribution between disc and pad in this work is calculated using standard formulae for heat partition coefficient [9].

Heat partition coefficient refers to the amount of heat generated which is “absorbed” by the disc and the amount “transferred” or “dissipated” to the pads and surroundings. Heat partition coefficient can be theoretically calculated for a thermal model according to Talati F. and Yevtushenko A. et. Al. as [9], [12]

$$\sigma_{\text{disc}} = \frac{\xi_{\text{disc}} A_{\text{disc}}}{\xi_{\text{disc}} A_{\text{disc}} + \xi_{\text{pad}} A_{\text{pad}}} \quad (16)$$

$$\sigma_{\text{Pad}} = 1 - \sigma_{\text{disc}} \quad (17)$$

where $\sigma_{\text{disc}}[-]$, $\sigma_{\text{Pad}}[-]$ are the disc, pad heat partition coefficients and are related as shown by equation (17) respectively, $A_{\text{disc}} [\text{m}^2]$ is the contact area of disc, $A_{\text{pad}} [\text{m}^2]$ is the contact area of pad and thermal effusivity ξ given in equation (16) is defined as the ability of a component to exchange thermal energy with the surroundings. Thermal effusivity ξ is calculated mathematically by equation (18) as [9]

$$\xi = \sqrt{k\rho c} \quad (18)$$

However, the response to the change in temperature is neglected in the empirical formulae [17]. In this work, the heat partition for the disc and pad is calculated as 98% and 2% respectively.

Brake power

Brake power is generated from brake torque. Brake torque is defined as the moment of braking force at the centre of rotating disc while, braking force is the tangential clamping force (the force of each pad against the disc) of friction acting at the brake disc and brake pad interface. The total power distribution in the brake system is described by the flow chart in Figure 2.8.

Total brake power P [W] on the wheel and brake torque T_b [N-m] are expressed in equation (19) and equation (20) as [18]

$$P = T_b \cdot \omega \quad (19)$$

$$T_b = 2 \cdot \mu \cdot p \cdot A_{\text{caliper}} \cdot r_{\text{eff}} \quad (20)$$

where T_b [N-m] the braking torque is defined as the braking force moment at the centre of the rotating brake disc, μ [-] is coefficient friction between brake

disc and brake pad, p [Pa] is the pressure applied on the wheel, $A_{caliper}$ [m²] is area of caliper, r_{eff} [m] is effective radius and ω [rad.s⁻¹] is the angular velocity of the wheel.

The pressure at the front and rear axle are test case dependent meaning that they differ for different braking manoeuvres. The detailed derivation of brake power is explained in brake technology handbook [18].

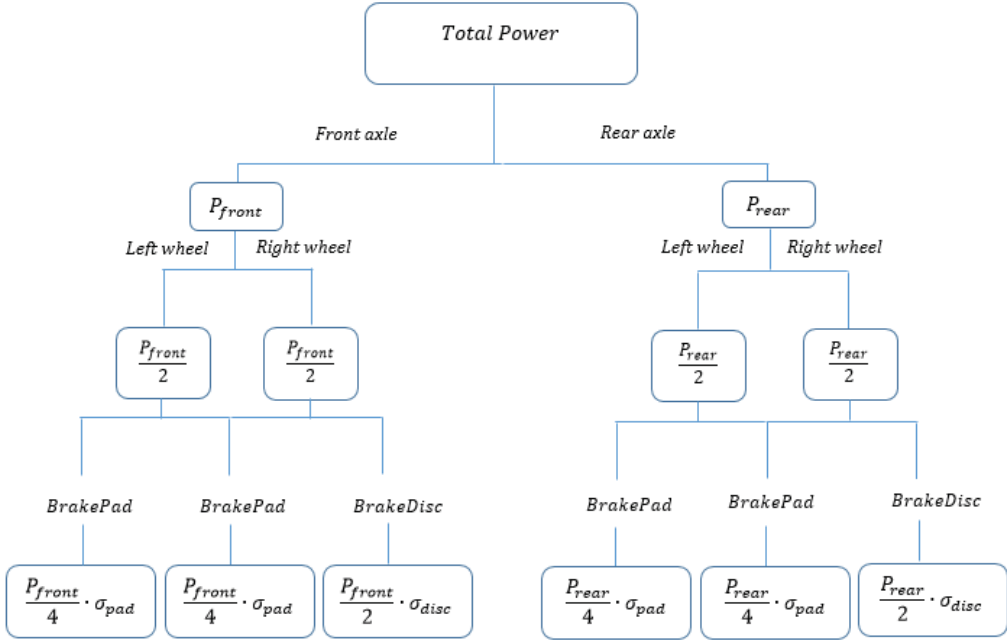


Figure 2.8. Brake power distribution flowchart.

Disc Temperature

As the angular velocity of the wheel increases, the brake disc temperature evenly spreads across the circumferential direction. The brake disc absorbs the maximum amount of brake energy. This energy input conducts through the brake disc and is dispersed to air by convection and radiation. The process of heat input and emission are a bit complex in reality depending on aerodynamics of the hub and type of disc explained by Thuresson A. [19].

Disc heat input. Input heat flux to the disc Q [W.m⁻²] given by equation (21) is calculated using brake power acting on the brake disc surface, heat partition coefficient of the brake disc, brake disc geometry and area of

friction contact. The mathematical equation is given by Pevec M. et al. as [20]

$$Q_{disc\ front/rear}(t) = \frac{\sigma_{disc} \cdot P_{front/rear}}{2 \cdot Area_{friction}} \quad (21)$$

where $P_{front/rear}$ [N.m⁻²] is the braking power at the front or rear axle and $Area_{friction}$ [m²] is the area of the friction surfaces *i.e.* the interface between the pad and disc surfaces during braking.

The frictional area is calculated from the brake pad geometry, see Figure 2.9. As there are two pads acting against the brake disc, the expression for area of friction surface is doubled and is given as

$$Area_{friction} = 2 \cdot \pi(r_3^2 - r_2^2) \quad (22)$$

where r_3 [m] and r_2 [m] are the outer and inner radius of the friction ring respectively

Disc heat output. Convection heat transfer is predominant in the brake disc at high speed (forced convection). According to Newton's law of cooling the heat loss is prescribed in equation (23) as

$$Q_{convection} = h \cdot Area_{friction} \cdot (T - T_{\infty}) \quad (23)$$

where $Area_{friction}$ [m²] is calculated from equation (22).

The other mode of heat dissipation is radiation, which according to [5] is estimated from equation (24) as

$$Q_{radiation} = \varepsilon \cdot Area_{disc} \cdot \sigma \cdot (T^4 - T_{\infty}^4) \quad (24)$$

In addition to the heat dissipation through convection, there is also radiation from the pad and the back plate that affects the disc.

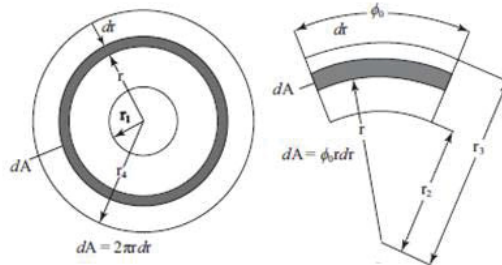


Figure 2.9. Contact surface element in disc (left) and pad (right) [9].

Pad Temperature

Conduction of the incoming heat during and after braking passes through the pad surface into the back plate. Heat is further conducted through to the calipers via the metal back plate of the pads. The function of the shim is to insulate the piston and mitigate noise during friction contact. It is composed of layers stacked with rubber and metal. The back plate has higher conductivity and hence enhances heat transfer. Heat is also radiated to the surroundings [5].

When observed microscopically, the sliding friction contact between the pad and disc results in limited pressurized contact points at the friction contact at each time instant. Such areas spread nominally over the entire disc surface during braking action. These limited points have temperature effect forming hot spots [5].

Pad heat input during braking. Input heat flux to the pad follows on the similar lines to that of the brake disc. The equations are formulated for the pad as below:

Input heat flux Q [$\text{W}\cdot\text{m}^{-2}$] to the pad is expressed in equation (25)

$$Q_{pad\ front/rear}(t) = \frac{\sigma_{\text{Pad}} \cdot P_{\text{front/rear}}}{4 \cdot \text{Area}_{\text{pad}}} \quad (25)$$

Pad heat input after braking. A major influencer in heat dissipation from the pad surface during the cooling phase is radiation [21]. The heat exchange [5] from the disc to the pad in the form of radiation given by equation (26) is

$$Q_{\text{abs,pad}} = \alpha_{\text{pad}} \cdot F_{\text{ij}} \cdot Q_{\text{radiation}} \quad (26)$$

where $Q_{\text{radiation}}$ [$\text{W}\cdot\text{m}^{-2}$] is the total heat radiation from energy absorbed by the pad, α_{pad} [-] is the percentage of energy absorbed by the brake pad whose magnitude is 30 % [5]. F_{ij} is the ratio of pad front surface area to the total disc surface area, expressed by equation (27) as

$$F_{\text{ij}} = \frac{\text{Area}_{\text{pad}}}{\text{Area}_{\text{disc}}} \quad (27)$$

Pad heat output after braking. Heat is dissipated from the pad by means of conduction to the caliper and combined effect of convection and radiation to the surrounding air.

Fluid/Caliper Temperature. The back plate, shim and the piston conduct heat from the pad during and after the braking action. The heat “spreads” into the piston hose and to the area surrounding the calipers. The heat inflow from the back plate through conduction is spread to the surrounding air from the caliper by convection and radiation. Also there is heat input through radiation from the disc.

Brake caliper model. The interface between the brake pad and caliper comprises of the back plate, shim and piston. However, since it is difficult to have the shim, caliper in an axisymmetric model, a rough estimate for shims and caliper is considered in the form of a simple axisymmetric rectangular block to mimic the thermal behaviour. For calibration, the conductivity of the caliper is adjusted to correlate with the experimental data.

2.5 Simulink Implementation

Simulink is a block diagram based tool for analysing multi domain dynamic systems. It has block libraries for simulating dynamic systems and is integrated within Matlab. Matlab allows importing models into Simulink and exporting results from it for further analysis. In the present work, the thermal model of brake disc is implemented in Simulink so that it can be integrated with other already in-house developed models in VCC for complete virtual vehicle simulations. The model consists of block diagrams for power input, brake disc and brake pad heat partition as shown in Figure 2.10.

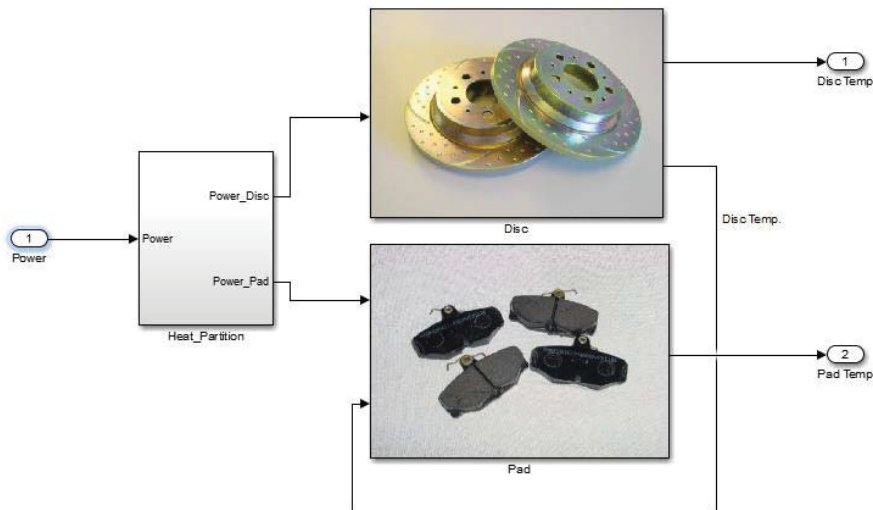


Figure 2.10. Block diagram of brake disc thermal model in Simulink

The combination of these blocks is used to calculate the output temperatures on the disc and pad surfaces. The s-function block is used to link the code written in Matlab to the Simulink model. Within the s-function block there are four sub categories: Setup, Start, Output and Update.

Setup block: The setup up block contains information about the number of input and output parameters, dimensions of geometry. Constant parameters necessary for the temperature calculation are given as a graphic user interface (GUI).

Start block: Start block controls model initialization. The block comprises creation of geometry, stiffness matrix, capacity matrix and incorporation of convection and radiation boundaries into the model.

Output block: In the output block, the temperatures of the disc and pad are calculated using the axisymmetric finite element equations. While radiation is a function of temperature and has to be updated at each instant of time, the radiation heat calculations are a part of this block.

Update block: This block updates the initial temperature obtained from previous time step for the each time instant during the transient analysis.

3 Calibration and Verification

3.1 Commercial Software

Initial investigation involved two test cases: transient heat transfer analysis on an axisymmetric model with rectangular and simplified brake disc cross sections. The test cases are created to check for accuracy of FE Matlab scripts. Abaqus FE solver is used as a validation of the two test cases.

Case 1:

The model considers a rectangular block with the following boundary conditions:

- a) Heat flux at one edge,
- b) Convection and radiation at adjacent edges.

The material properties for the transient analysis are stated in Table 3.1.

Table 3.1. Parameters for transient analysis

Parameter	Magnitude
Heat flux	10^6 Wm^{-2}
Convective coefficient	$15 \text{ Wm}^{-2}\text{K}^{-1}$
Emissivity	0.5
Ambient temperature	20 °C
Initial temperature	527 °C

The rectangular model is simulated for a time period of 10 seconds. Heat flux is given at the top boundary, see Figure 3.1 while linear triangular elements are used for the transient analysis. The scale in Figure 3.2 represents the temperature gradient across the geometry at the end of the braking cycle, *i.e.* 10 seconds. While there is convection and radiation at the adjacent boundaries in the heating phase, heat dissipation occurs at all boundaries excluding the symmetry line during cooling phase.

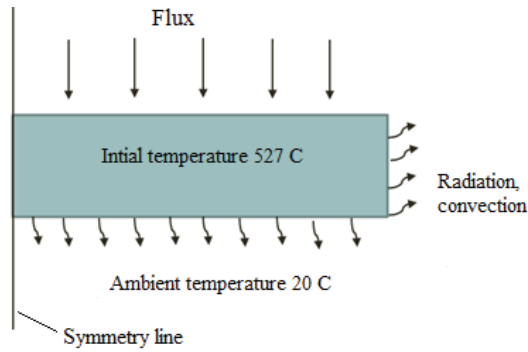


Figure 3.1. Axisymmetric rectangular block undergoing heat dissipation via three modes of heat transfer.

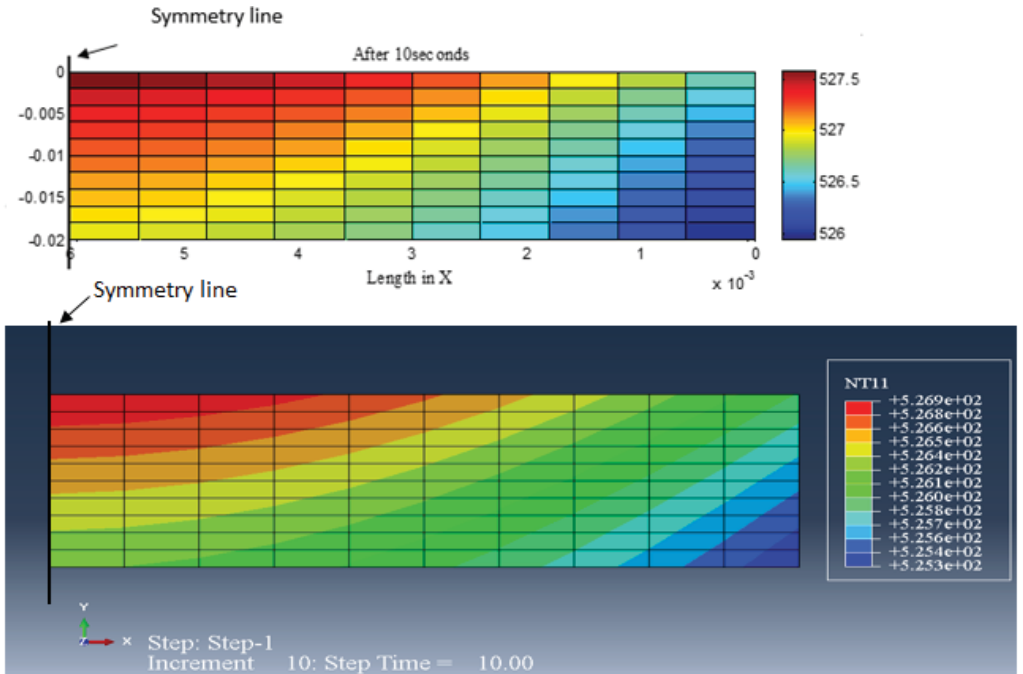


Figure 3.2. Transient heat model undergoing convection and radiation heat transfer on an axisymmetric rectangle from both MATLAB (above) and ABAQUS (below). Note the temperatures mentioned in the axis are in Kelvin scale.

Case 2:

The axisymmetric model with simplified brake disc geometry is evaluated in the second case. The same material properties as Table 3.1 are used in this case. The heat flux is imposed on two edges as shown in Figure 3.3 for a period of 5 seconds. Heat dissipates from all edges (including regions of imposed heat flux) during the transient analysis. The nodal temperatures tabulated in Table 3.2 computed from Matlab and Abaqus models correlate with a good level of agreement as observed in Figure 3.4, Figure 3.5 and Figure 3.6.

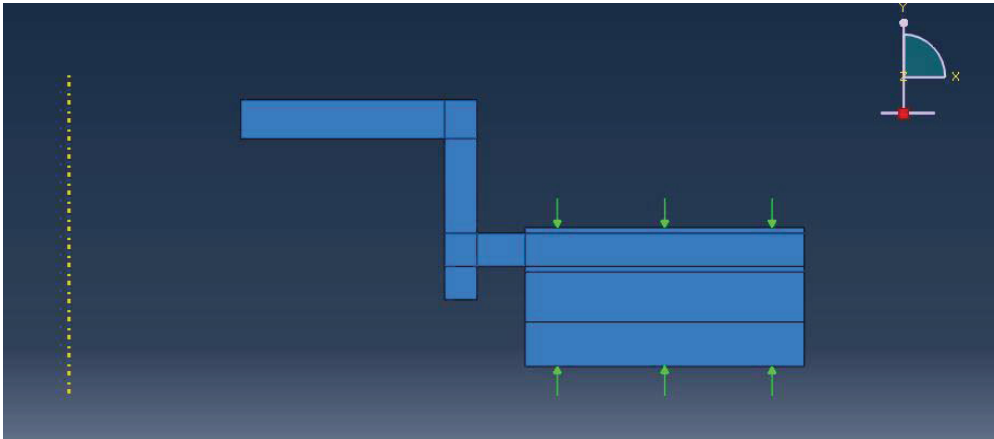


Figure 3.3. Indicates brake disc with the regions of imposed heat flux boundary.

Results of the transient analysis:

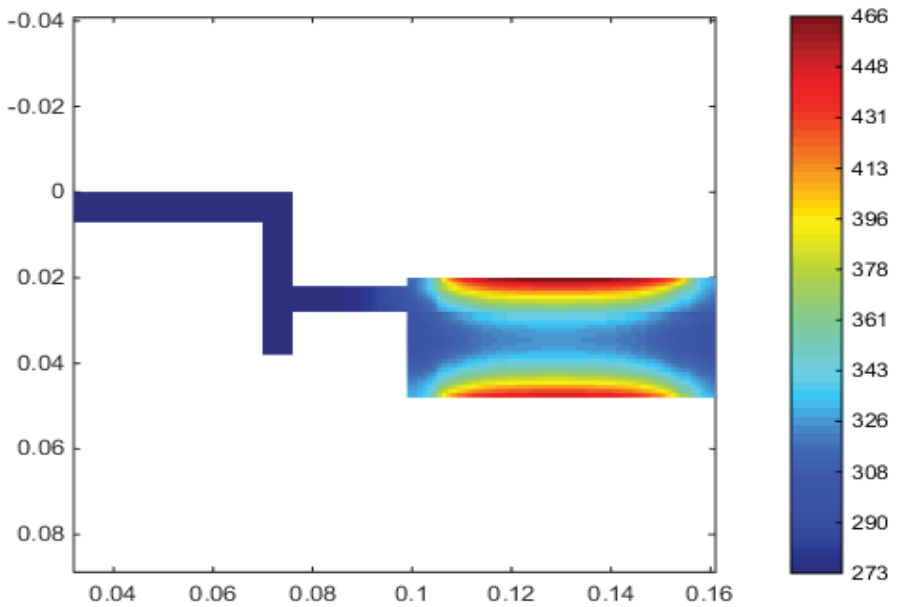
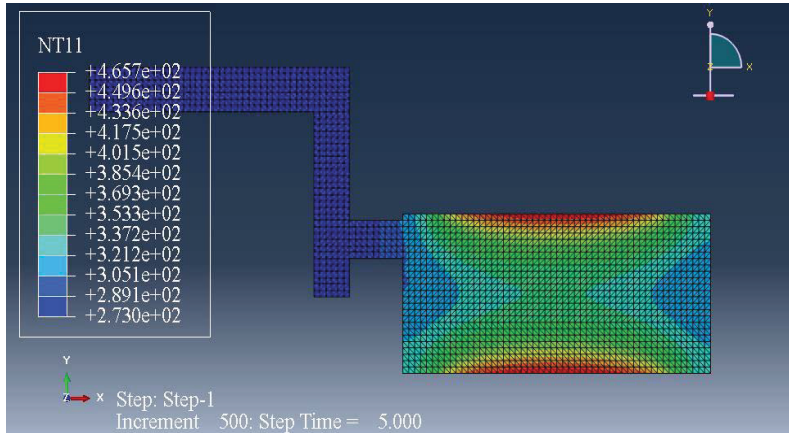


Figure 3.4. Transient analysis with convection and radiation during heating phase at time $t=5$ s in Abaqus (above) and Matlab (below). Note that the temperatures mentioned in the axis are in Kelvin.

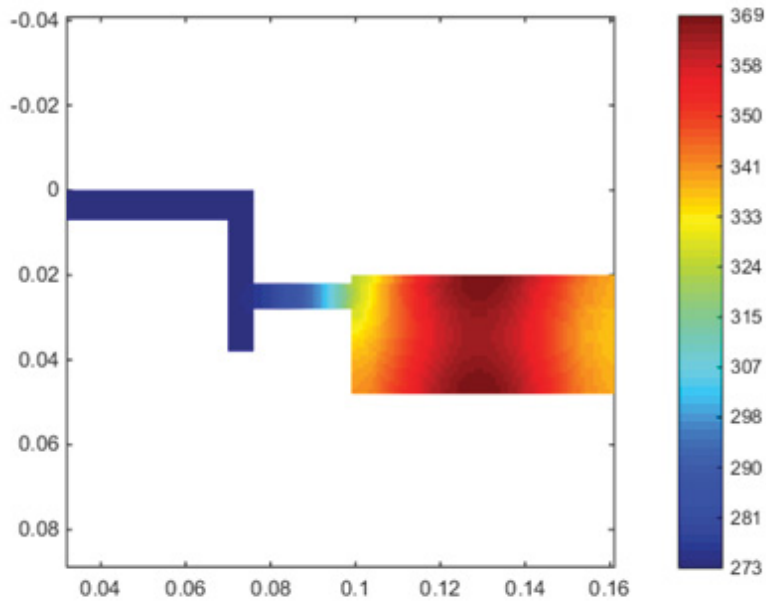
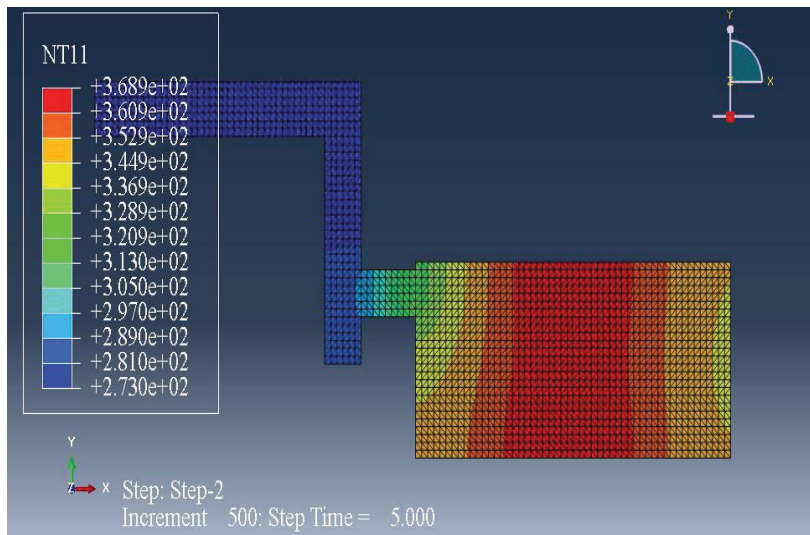


Figure 3.5. Transient analysis with convection and radiation during heating phase at time $t=10$ s in Abaqus (above) and Matlab (below). Note the temperatures mentioned in the axis are in Kelvin.

Table 3.2. Temperature evolution table for the transient analysis.

Time step(sec)	Maximum Temperature			
	Heating phase [K]		Cooling phase [K]	
	Matlab	Abaqus	Matlab	Abaqus
1	358	357.9	401	402
2	394	393.4	386	385.2
3	421	420.7	377	377
4	445	444.2	373	372.2
5	467	465.7	370	368.9

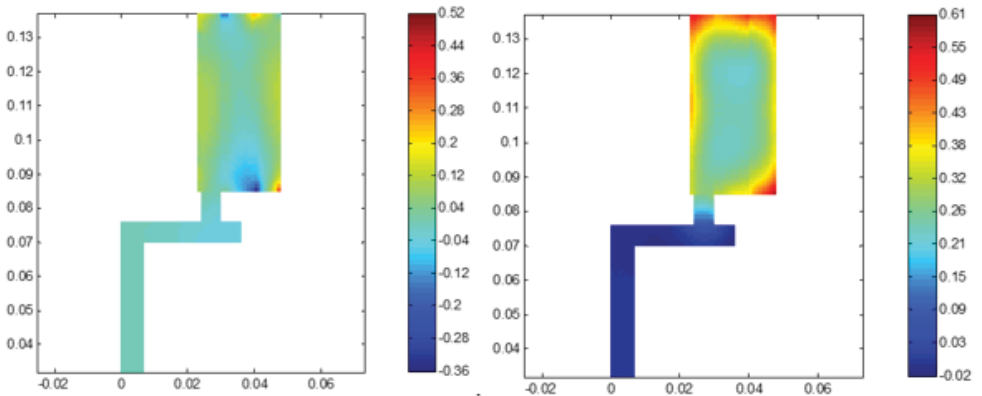


Figure 3.6. Nodal temperature difference between Matlab and Abaqus model at the end of the heating phase (left) and at the end of the cooling phase (right).

3.2 Measurement

Test procedure description

The tests are performed at VCC test tracks in Gothenburg. Thermocouples are used to record temperature evolutions on the brake disc and brake pad surfaces. Thermocouples are devices that measure temperature by correlating voltage difference between the junction of two metal alloys against a reference voltage. They are made of two thin metal wires welded to form a junction. The reason for their widespread application is that they can withstand large temperature gradients. To measure the temperature at the

brake disc and brake pad surfaces, class 1 thermocouple of type K is used which has a tolerance of ± 3.2 °C for temperatures around 800 °C. Accurate measurements require the thermocouple wires to remain isolated to avoid short circuit. A short circuit between the uninsulated thermocouple wires causes deviation from the measurement point resulting in errors. For the test cases, thermocouples are embedded as close as possible to the centre of the pad as seen in Figure 3.7. Likewise, thermocouples are embedded at a distance of 2 mm below the brake disc surface at the effective radius of the disc, see Figure 3.8.



Figure 3.7. Position (marked by red circles) of thermocouples on the front (left) and rear (right) pads.

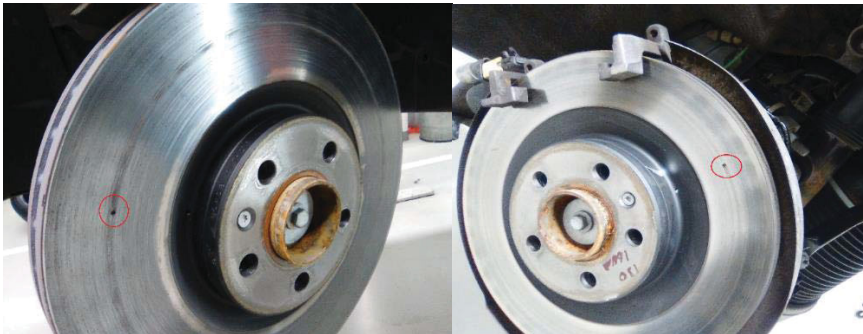


Figure 3.8. Position (marked by red circles) of thermocouples embedded at a distance of 2mm inside the front (left) and rear (right) disc.

Results

In the following, the calibration of the FE thermal model with the test data for three different load cases are presented. The developed Matlab toolbox for thermal brake dimensioning is generic for calculating brake disc temperatures independent of the load case. Since the airflow around the wheel base on the front and rear axle changes for different vehicles and at different speeds, the values for convection coefficient and emissivity are calibration based in the current work. The results of the model based calibration are chosen to be conservative, *i.e.* over predicting the temperatures. The calibration values for convective heat transfer coefficient and emissivity are tabulated under each test case respectively. The calibrated measures are load case dependent. The brake power distribution between the front and rear axle is calculated from the pressure given in the test data. The mathematical relation to estimate the brake power distribution from the pressure on the brake pedal is given by equation (20).

Test case I: 10 consecutive brake cycles

The test consists of 10 successive stop braking from 130 km.h⁻¹ or 110 km.h⁻¹ to a full stop with a maximum deceleration of 11 [m.s⁻²]. The calibration parameters for Test case I are shown in Table 3.3. The results show good agreement between experiments and simulation for the brake disc and brake pad as observed in Figure 3.9 and Figure 3.10 respectively. The calibration parameters mentioned in Table 3.3 are applicable for the Test case having the same speed range irrespective of the change in geometry of the brake disc and brake pads.

Table 3.3. Parameters for the calibration of Test case I.

Parameter	Front axle		Rear axle	
Brake power distribution	80 %		20 %	
Heat distribution at the friction contact	98 % to disc and 2 % to the pads		98 % to disc and 2 % to the pads	
	Heating phase	Cooling phase	Heating phase	Cooling phase
h_{disc} [Wm ⁻¹ K ⁻¹]	60	90	30	60
h_{pad} [Wm ⁻¹ K ⁻¹]	20	40	10	30
ϵ [-]	0.6	0.6	0.6	0.6

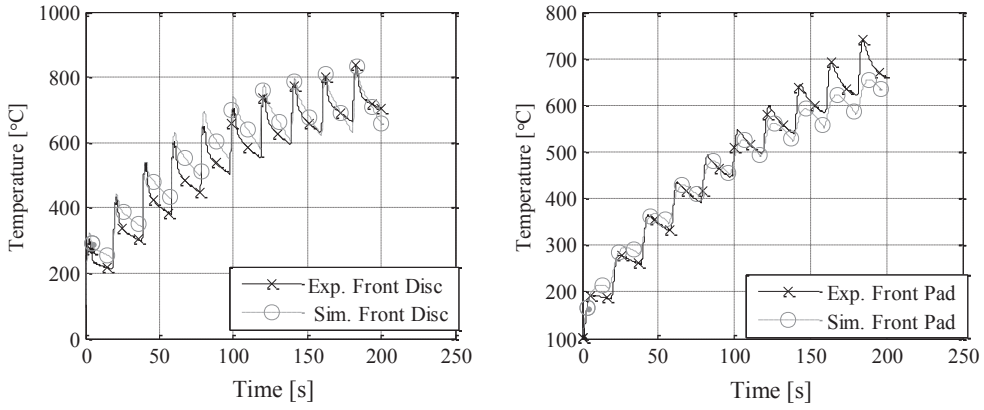


Figure 3.9. Test Case I calibration (Sim) and experimental (Exp) temperature results for the front disc (left) and the front pad (right). Note the different temperature scales for the vertical axis.

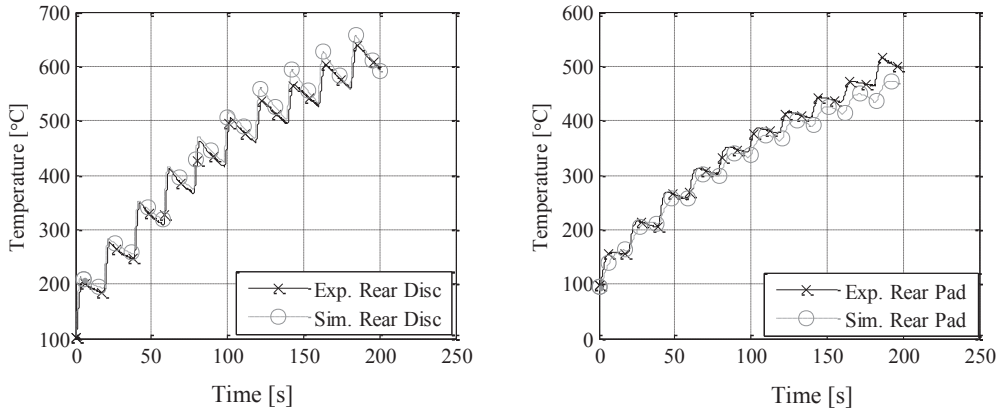


Figure 3.10. Test Case I calibration (Sim) and experimental (Exp) temperature results for the rear disc (left) and the rear pad (right). Note the different scales on the vertical axis.

Test Case II: High-speed deceleration

The test consists of 15 braking with a deceleration at 6 m.s^{-2} on a half loaded vehicle, from 90 % of the maximum speed to 90 km.h^{-1} . The calibration parameters are tabulated in Table 3.4. In Figure 3.11 and Figure 3.12, you can observe a sudden rise in temperature for alternate brake cycles. These are due to the formation of hot spots, which produce localized high temperatures by virtue of uneven pressure distributions at the contact interface of brake disc and brake pads [22]. Since the axisymmetric model cannot capture this phenomenon, the temperatures for this Test case are calibrated to the maximum temperatures.

Table 3.4. Parameters for calibration of Test case II.

Parameter	Front axle		Rear axle	
	Heating phase	Cooling phase	Heating phase	Cooling phase
Heat distribution at the friction contact	98 % to disc and 2 % to the pads		98 % to disc and 2 % to the pads	
$h_{\text{disc}} [\text{Wm}^{-1}\text{K}^{-1}]$	70	120	70	120
$h_{\text{pad}} [\text{Wm}^{-1}\text{K}^{-1}]$	30	60	20	50

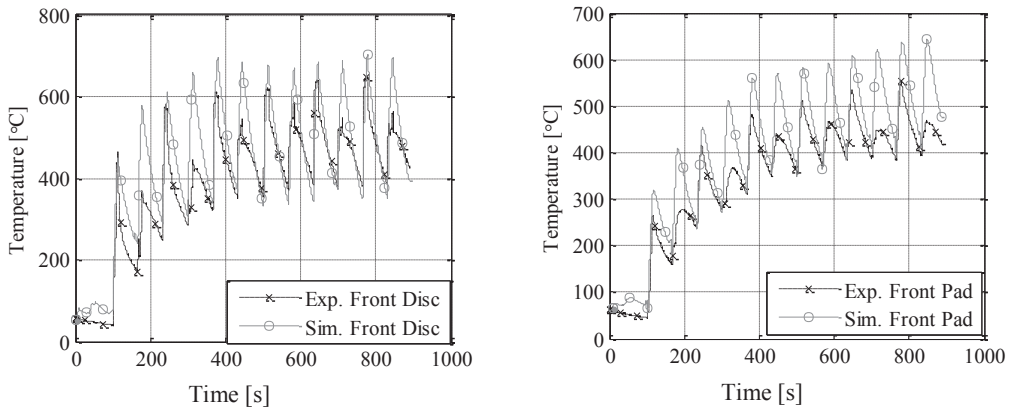


Figure 3.11. Test Case II calibration (Sim) and experimental (Exp) temperature results of the front disc (left) and the front pad (right). Note the different scales on the vertical axis.

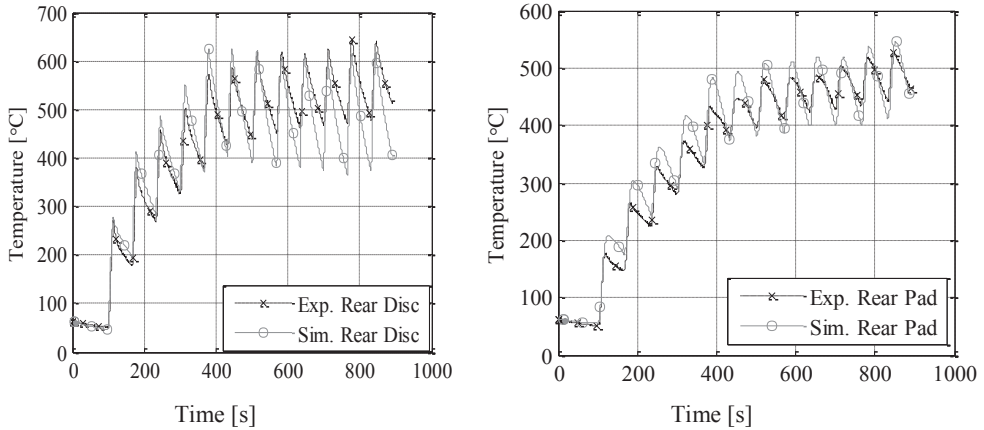


Figure 3.12. Test Case II calibration (Sim) and experimental (Exp) temperature results of the rear disc (left) and the rear pad (right). Note the different scales on the vertical axis.

Test Case III: Downhill braking

This test consists of drag braking at a constant speed on a 10 % slope for about 50 minutes. Drag braking is of longer duration as compared to the previous two test cases. Material properties and calibration parameters are shown in Table 3.5 and Table 3.6.

Figure 3.13 and Figure 3.14 show the temperature evolution in the brake disc and brake pad at the front and rear axle for Test Case III. The experimental temperature of the brake fluid at the rear axle in Figure 3.15 has a dip in temperature. The reason for this could be faster cooling of the rear since it has low energy accumulated than the front as a result of less braking action. Since the caliper at the front and rear axle should be calibrated with the same parameters, the calibration is conservative in case of the rear fluid temperature.

Table 3.5. Material properties of brake disc system.

Parameters	Disc	Pad	Caliper
Density [$\text{kg}\cdot\text{m}^{-3}$]	7200	2000	7200
Conductivity [$\text{Wm}^{-1}\text{K}^{-1}$]	48	2	15
Specific heat [$\text{Jkg}^{-1}\text{K}^{-1}$]	540	1000	540

Table 3.6. Parameters for calibration of Test case III.

Parameter	Front axle		Rear axle	
	Heating phase	Cooling phase	Heating phase	Cooling phase
Heat distribution at a friction contact	98% to disc and 2% to the pads		98% to disc and 2% to the pads	
h_{disc} [$\text{Wm}^{-1}\text{K}^{-1}$]	10	40	10	40
h_{pad} [$\text{Wm}^{-1}\text{K}^{-1}$]	2	25	2	25
$h_{\text{brake fluid}}$ [$\text{Wm}^{-1}\text{K}^{-1}$]	-	2	-	2

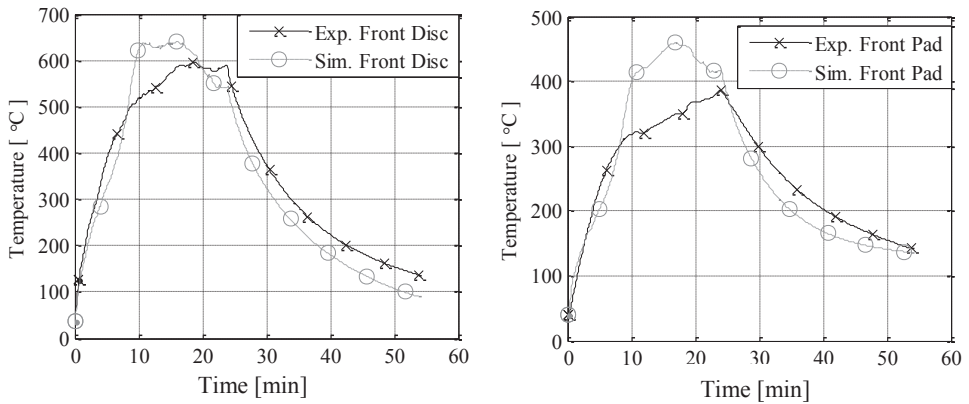


Figure 3.13. Test Case III calibration (Sim) and experimental (Exp) temperature results of front brake disc (left) and the front brake pad (right). Note the different scales on the vertical axis.

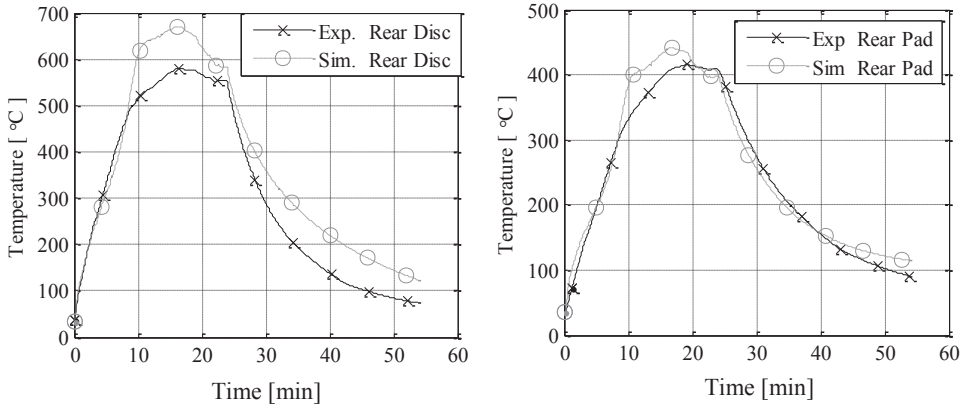


Figure 3.14. Test Case III calibration (Sim) and experimental (Exp) temperature results of the rear brake disc (left) and the rear brake pad (right). Note the different scales on the vertical axis.

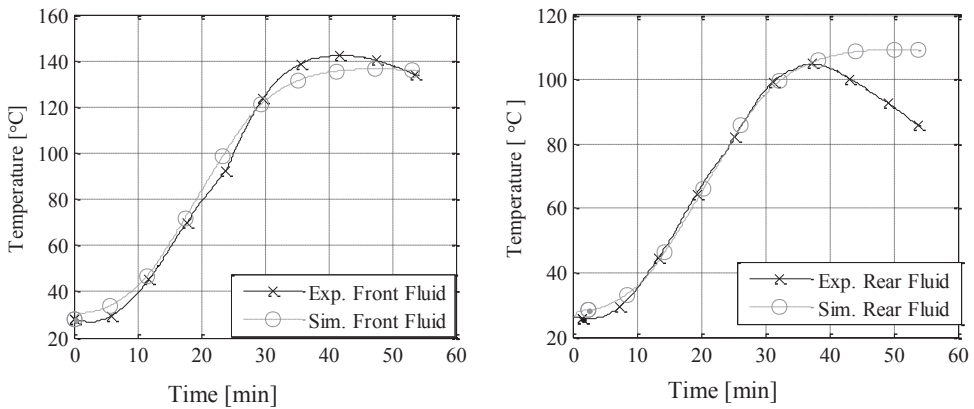


Figure 3.15. Test Case III calibration (Sim) and experimental (Exp) temperature results of brake fluid at the front axle (left) and rear axle (right). Note the different scales on the vertical axis.

3.3 Sensitivity analysis

Sensitivity analysis is carried out for Test Case I: 10 successive braking to understand the significance of change in emissivity and convection coefficient while braking and acceleration.

Case 1:

Two tests are carried out with calibrated convection coefficients from experimental data, *i.e.* convection coefficient, while braking $h_b = 60$, convection coefficient while accelerating $h_a = 90$.

Test (a): Having h_a constant while increasing and decreasing h_b by 50 %

Test (b): Having h_b constant while increasing and decreasing h_a by 50 %

Table 3.7 and Table 3.8 show the effect of increasing h_b by 50 % while h_a is constant and vice versa. The convection coefficient during acceleration h_a is more sensitive and has a change in temperature of around 16 % as compared to the convection factor during braking h_b . The elaborate effect of change in parameters on temperature can be observed in Figure 3.16.

Table 3.7. Percentage change in temperature for test Case I Test (a).

h_a (convection coefficient while accelerating)	h_b (convection coefficient while braking)	Maximum Temperature[°C]	Percentage change in temperature:
90	60 (reference)	815	NA
90	90 (increased by 50 %)	792	-2.8 %
90	30 (decreased by 50 %)	840	+3 %

Table 3.8. Percentage change in temperature for test Case I Test (b).

h_b (convection coefficient while braking)	h_a (convection coefficient while accelerating)	Maximum Temperature [°C]	Percentage change in temperature:
60	90 (reference)	815	NA
60	135 (increased by 50 %)	705	-13.5 %
60	45 (decreased by 50 %)	946	+16 %

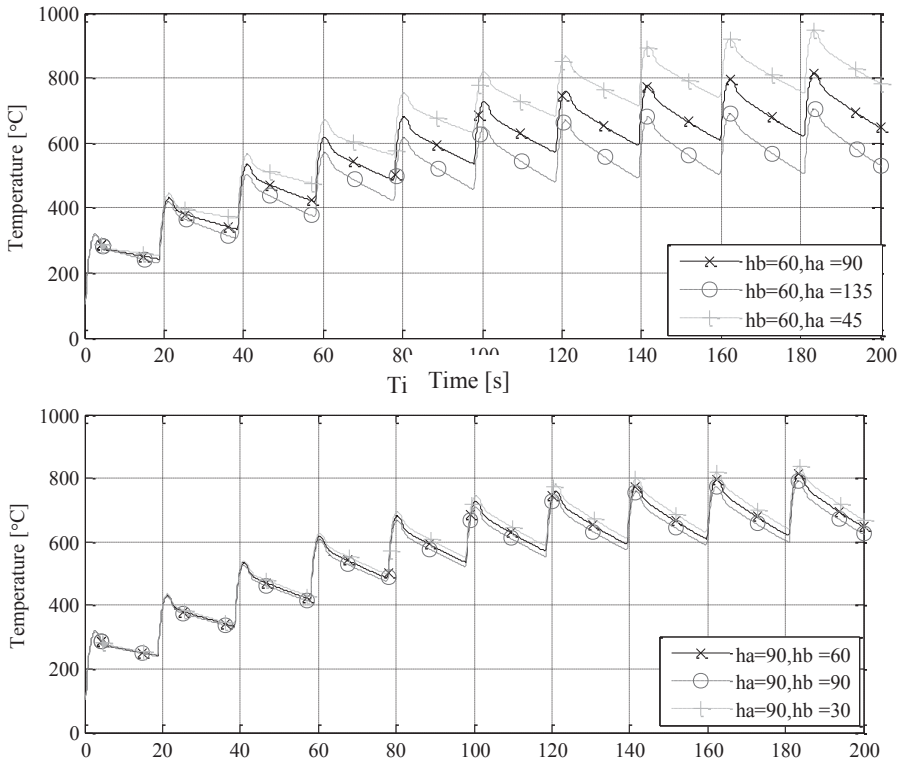


Figure 3.16. Sensitivity analysis correlation with convection coefficient while braking and accelerating with $h_a = 90$ and $h_b = 60$.

Case 2:

Two tests are carried out by changing the original emissivity from experimental data, *i.e.* $\varepsilon = 0.6$.

Test (c): increasing ε by 50 %

Test (d): decreasing ε by 50 %

Table 3.9 shows the percentage influence in temperature with change in emissivity. From Figure 3.17 we can observe the difference with change in emissivity as the temperature increases because of influence of radiation at higher temperatures.

Table 3.9. Percentage change in temperature for test Case 2.

Emissivity	Maximum Temperature[°C]	Percentage change in temperature:
0.6 (reference)	815	NA
0.9 (increasing ε by 50 %)	788	-3.3 %
0.3 (decreasing ε by 50 %)	850	+4.3 %

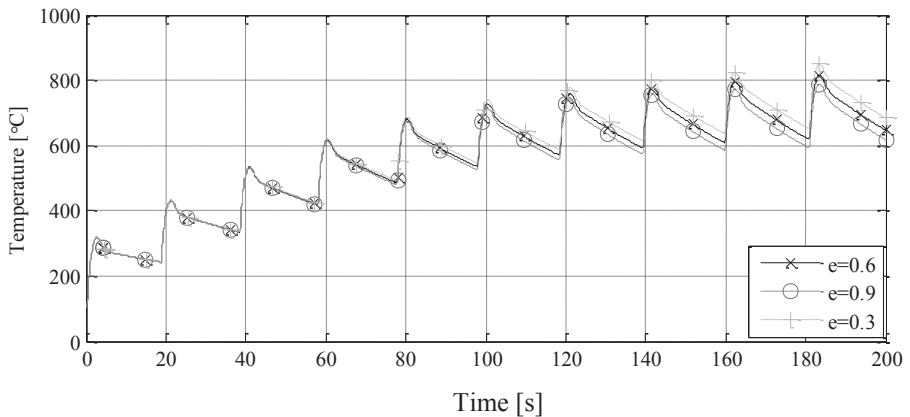


Figure 3.17. Sensitivity correlation compared with emissivity 0.6.

4 Discussion and Conclusion

A FE toolbox able to run thermal brake dimension calculations has been proposed and implemented. The work presents modelling approach, power distribution and calibration of simulation results with respect to experimental data. The axisymmetric brake disc and brake pad thermal model has a good correlation with the experimental test data as observed in the results. The questions addressed in the research are outlined as follows

1. What is the influence of braking manoeuvres on brake disc and brake pad temperatures?
 - The research has considered three specific severe test cases which are critical in the context of brake dimensioning. The test cases are namely: *10 consecutive brake cycles*, *High speed deceleration* and *Downhill braking*. As observed in the *10 consecutive brake cycles* test, vehicle undergoes maximum deceleration when compared to the other two test cases *i.e.* the brake energy at the front axle is greater thereby resulting in greater heat generation at the front wheels than the rear. Hence, temperature evolution on the brake disc at the front is higher. While, in the case of *High speed deceleration* and *Downhill braking*, the brake energy distribution at the front and rear are balanced leading to quite similar temperature fields at the front and the rear axles.
 - Temperature graphs in the case of *High speed deceleration* show the effect of hot spots and banding, a phenomenon prominent during braking action at higher speeds. This behaviour is observed by the rise and drop of temperatures during consecutive brake cycles. Banding and hotspots form on brake disc surfaces due to sliding friction, thermal expansion and disc thickness variation involving contribution from residual stresses to an extent. Hotspots produce high localized temperature effects and sometimes appear at the disc mid radius while having a shift in their position for different brake cycles. These hotspots move in the direction opposite to the brake disc rotation. Since the axisymmetric thermal model cannot capture hot spotting, brake

disc and brake pad temperatures have been calibrated to the maximum temperatures.

- For obtaining brake fluid temperatures, the thermal brake disc model was extended using a rectangular block. The reason for a dip in brake fluid temperature at the rear axle is due to low brake energy stored as a result of less braking action which is dissipated during vehicle acceleration. Overall, the temperature fields during different braking manoeuvres are a consequence of vehicle speed and heat distribution transferred due to the braking action which we have successfully captured with the help of an axis symmetric model. In addition, the brake disc model can be calibrated using the magnitudes for heat coefficient during braking, heat coefficient during acceleration and emissivity tabulated in this work for different braking actions irrespective of the vehicle type or brake disc geometry (16, 17, 18 or 19-inch brake disc).
2. What is the influence of temperature and velocity on heat dissipation coefficients?
- The brake disc cooling is a complex phenomenon governed by Fourier's law occurring on the lines of the three heat transfer modes namely conduction, convection and radiation. The heat dissipation is based on several factors such as vehicle speed, temperature, aerodynamics of the wheel and design of the wheelbase. The aerodynamics around the wheel base shows complex behaviour depending on the design of the wheel base, air flow and vehicle velocity. There are instances when the air flow is blocked due a certain design of the wheel base and vice versa. The thermal model has accounted for these phenomena during calibration by changing the emissivity and convective heat transfer coefficients respectively. However, emissivity and convection heat coefficient could be made temperature and velocity dependent to improve the model accuracy. Another ideology could be to run an optimization experiment with the temperature and velocity dependent factors with the objective of minimizing the area under the curve. Apart from the approximations in the thermal model, there are possible sources

of error during vehicle testing as well such as technical error in thermocouples, incorrect placement of the sensors etc.

An interesting observation with respect to the sensitivity analysis as observed in the graph showcasing the effect of change in emissivity with the brake temperatures is the prominence of emissivity at higher temperatures.

3. How to handle brake fluid temperatures in an axisymmetric model?

- The thermal model is extended to measure brake fluid temperatures to ensure that no vaporization can occur as temperature propagates via the pads to the caliper. A rectangular block is modelled with the pad for the temperature of the brake fluid as an approximation for the piston and surrounding components which would otherwise be a complex task in case of an axisymmetric model. Therefore, a rough estimate in the form of a rectangular block is used to obtain the brake fluid temperatures. It is observed that even though the brake fluid is calibrated for maximum temperatures, we observe that the fluid temperature is well within the bounds of evaporation.

In addition to the questions raised in the research, other aspects of interest which have come to light are also presented.

- The consideration of axis symmetry has a drawback. In reality, there is banding and hotspot formation on the disc surface. Banding and hotspots form on brake disc surfaces due to sliding friction, thermal expansion and disc thickness variation involving contribution from residual stresses to an extent. Hotspots produce high localized temperature effects and sometimes appear at the disc mid radius while having a shift in their position for different brake cycles. These hotspots move in the direction opposite to the brake disc rotation. Though, the axisymmetric model can capture uniform surface banding, it is impossible for the model to handle hot spots and replicate the realistic brake disc cooling channels.
- Design of the thermal model has the effect of vanes in the brake disc incorporated by having convection and radiation boundaries at the section separating the two disc surfaces on the hat and piston side. In addition, the section is given a reduced specific heat value. The cooling effect of vanes from the experiments is

calibrated using the combined effect of change in specific heat of the section and convective heat coefficient, emissivity. More investigation can be laid on the design of vanes in the model to predict accurate cooling curves.

- The quality of a mesh and a robust solver play an important role in predicting the accuracy of a solution. Rate of convergence depends on mesh quality, with accuracy increasing as the mesh size decreases. The mesh size considered for the brake disc and brake pads are 1mm and 0.5 mm respectively. The mesh quality is considered based on compatibility with adjacent boundaries and heat propagation across and within elements. The use of triangular elements are suitable in case of finite element problems having complex geometries and discontinuities along the calculation domain. Another aspect concerning the FE analysis is its computational time. It is important to have a balance between solution accuracy and computation time requiring the code to be as robust as possible. The computed performance-cost ratio for the considered test cases are 0.25, 0.25 and 10.41 for Test Case I, Test Case II and Test Case III respectively. A performance-cost ratio below 1 is common, for any ordinary solver takes more time to compute compared to the real test while, if the ratio is greater than 1, the simulation performance has good credibility.
- Power distribution is calculated from the pressure on the brake pedal by decoupling the brake pad and brake disc system, *i.e.* the thermal model has the heat flux distribution controlled by the user. The introduction of a so called third body layer into the model will be an effective way to have thermal continuity between the disc and pad interface based on their material properties respectively. In addition, the heat is assumed to be distributed equally on the disc surface, on both sides (hat side and piston side) in the brake disc model. However, in reality, the temperature on the disc surface at the hat side is slightly (around 10 %) higher than the temperature on the piston side. This difference in temperature is due to thermal distortion of the brake disc known as coning which occurs due to uneven distribution of temperature on the brake disc and brake pad surface. The coning can be taken into account by having a full scale 3-D model.

The brake disc thermal model in this work is a fundamental tool in brake dimension development. The axisymmetric brake disc FE model has a good correlation with the test cases examined. This justifies the use of an axisymmetric model for performing brake dimension calculations in future. The above outlined practical limitations in the model could be studied by making a transformation towards a 3-D model. However, a switch to a full scale 3-D model will require the use of high computational resources and time.

5 Future Work

For the improvement of the brake disc thermal model, there are possible developments which could be beneficial to have. Six suggestions for model improvement are outlined as follows

- *Temperature and velocity dependent boundary conditions.* The current model has constant convection coefficient and emissivity factors around the whole geometry of the brake disc. For calibration these factors were tweaked based on test results. However, since the aerodynamics around the wheel base is a complex phenomenon, having the heat dissipation coefficients, temperature and velocity dependent would be of immense help to have better cooling characteristics in the model.
- *Implementation of realistic vane design.* The current brake disc model has a solid vane with hypothetical material properties to replicate the ventilated vane. However, a ventilated vane design demands a 3-D model and cannot be modelled with the current axisymmetric model. It would also be useful to study the effect of different vane designs on brake disc cooling.
- *Geometry import from ANSA/Beta CAE.* For the future CAE applications, a possible way to have the brake disc geometry as close as possible to the reality would be to create the mesh and geometry in ANSA or any other commercial FE solver and import it to Matlab/Simulink.
- *Modelling the thermal behaviour between the brake disc and brake pad.* The thermal interaction at the brake disc and brake pad interface is a complex phenomenon with hot spotting and banding effects. The process is complex and requires lot of computation time. Though the current model has good calibration tendency, it would be useful to have a 3-D model to study the thermoelastic instabilities like hot spotting.

- *Modelling the friction surface using third body layer.* The heat partition between the brake disc and brake pads are calculated using the test data. The use of third body layer at the friction contact would simultaneously account for the heat transfer depending on material properties of the brake disc and brake pad. The task of finding the material properties of the third body layer though is time consuming and requires a detailed study since it depends on a lot of conditions, but the process is worth the time.
- *Brake fluid model using thermal resistance.* Modelling the interface between the pad and caliper comprises the back plate, shims and piston which is tough to accommodate in an axisymmetric model. The brake fluid temperature was estimated by adjusting the conductivity of the rough rectangular block. The concept of thermal resistance would thus be an interesting addition in the full scale 3-D model.

6 References

- [1] D. Patrascu, “Braking Systems History,” *Autoevolution*, 2009.
- [2] “Disc vs. Drum Brake” *Animagraffs*, 2016.
- [3] “Brake Systems,” *Integrated Publishing*.
- [4] “Performance Brake Blog - Brake Rotor Vein Design Types and Considerations” *CQUENCE Performance Brake Parts*, 2012.
- [5] A. Neys, “In-vehicle brake system temperature model,” 2012.
- [6] J. Erjavec, *Automotive Brakes*. Cengage Learning, 2003.
- [7] G. Broman, *Computational engineering*. Blekinge Institute of Technology, Karlskrona, Sweden, 2003.
- [8] D. A. Secrist and R. W. Hornbeck, “An Analysis of Heat Transfer and Fade in Disk Brakes,” *J. Eng. Ind.*, Vol. 98, (2), pp. 385–390, May 1976.
- [9] F. Talati and S. Jalalifar, “Analysis of heat conduction in a disk brake system,” *Heat Mass Transfer*, Vol. 45 (8), pp. 1047–1059, Jan. 2009.
- [10] S. S. Rao, *The Finite Element Method in Engineering*. Elsevier, 2010.
- [11] P. Kythe and D. Wei, *An Introduction to Linear and Nonlinear Finite Element Analysis: A Computational Approach*. Springer Science & Business Media, 2011.
- [12] A. A. Yevtushenko and P. Grzes, “Axisymmetric FEA of temperature in a pad/disc brake system at temperature-dependent coefficients of friction and wear,” *International Communications in Heat and Mass Transfer*, Vol. 39 (8), pp. 1045–1053, Oct. 2012.
- [13] R. Eisengraber, J. Grochowicz, M. Schuster, K. Augsburg, and L. Koch, “Comparison of Different Methods for the Determination of the Friction Temperature of Disc Brakes,” 1999.
- [14] T. Chung, *Computational fluid dynamics*. Cambridge university press, 2010.
- [15] P. E. Austrell *et al.*, “CALFEM-a finite element toolbox, version 3.4,” 2004.
- [16] “Types of mesh - Wikipedia, the free encyclopedia.”
- [17] Y.-C. Yang and W.-L. Chen, “A nonlinear inverse problem in estimating the heat flux of the disc in a disc brake system,” *Applied Thermal Engineering*, Vol. 31 (14), pp. 2439–2448, 2011.
- [18] B. Breuer and K. H. Bill, *Brake technology handbook*. 2008.
- [19] A. Thuresson, “CFD and Design Analysis of Brake Disc,” *Chalmers University of Technology, 2014*, Vol. 2014:11.

- [20] M. Pevec, T. Lerher, I. Potrc, and D. Vranesevic, "Numerical temperature analysis of brake disc considering cooling," *Advanced Engineering*, Vol. 4 (1), pp. 55–64, 2010.
- [21] A. Vdovin, "Investigation of Aerodynamic Resistance of Rotating Wheels on Passenger Cars," *Chalmers University of Technology*, Gothenburg, Sweden, 2013.
- [22] G. Le Gigan, "On improvement of cast iron brake discs for heavy vehicles," *Chalmers University of Technology*, Gothenburg, Sweden, 196p, 2015.

7 Appendix

Creating a mesh geometry using CALFEM

To create a geometry and mesh, we have to define vertices coordinates, line segments from vertex index, and surfaces from the segment index.

Example:

1. Creating L shaped cross section shown in Figure 7.1 using CALFEM functions.

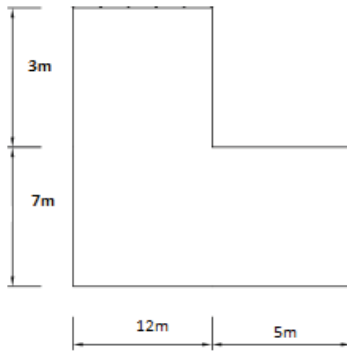


Figure 7.1. L-shaped cross-section

Identify all vertices and segments as in Figure 7.2,

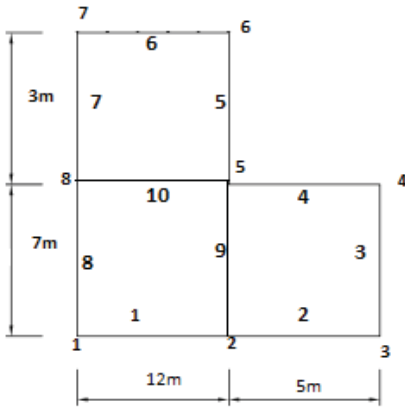


Figure 7.2. Element and node numbers defined for the cross-section

i.e., Vertices 1 and 2 makes line segment 1,
Vertex 2 and 3 makes line segment 2 and so on.

Now identify the surfaces from line segments index defined in Figure 7.3

i.e., Line segment 1, 9, 10, 8 makes surface 1
Line segment 2, 3, 4, 9 makes surface 2
Line segment 10, 5, 6, 7 makes surface 3

```

Vertices=[0 0
12 0
17 0
17 7
12 7
12 10
0 10
0 7]; % Defining Vertices coordinates( X ,Y)

Segments=[1 2
2 3
3 4
4 5
5 6
6 7
7 8
8 1
2 5
8 5]; % Defining the line segments from vertex index

Surfaces=[1 9 10 8
2 3 4 9
10 5 6 7]; % Defining the surfaces from segment index

```

Figure 7.3. Matlab geometry definition.

Next step is to define the element size on each line segment and mesh type (triangular or quadrilateral) shown in Figure 7.4,

```
Segp=[9 4 7 4 3 9 3 7 7 9];% Define number of element on each segment
nen=3; % traingular element =3, quadrilateral =4
dofspernode=1; % degrees per node
mp=[dofspernode, nen];
```

Figure 7.4. Element and mesh configurations in Matlab.

Now we create a geometry seen in Figure 7.5, using these vertices, segments, surfaces.

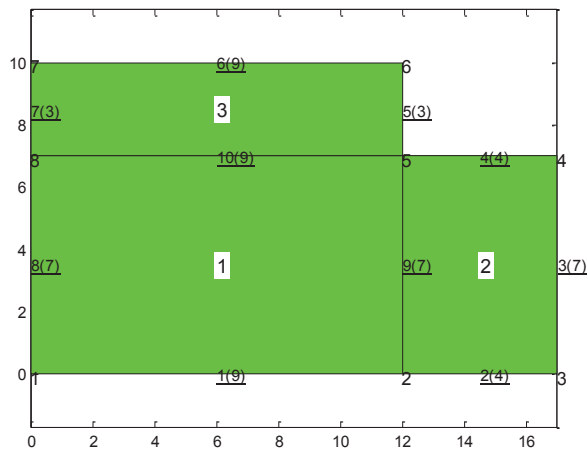


Figure 7.5. Geometry with boundary compatibility between sections.

Plot geometry using *geomdraw* function.

```
geomdraw2(Vertices,Segments,Surfaces,Segp,mp); % Drawing geometry
```

Next is to generate the element mesh and element coordinates.

These can be done using *strMeshgen* and *coordxtr* functions

```
[Coord,Edof,Dof,meshdb]=strMeshgen(Vertices,Segments,Surfaces,Segp,mp); % function to
Generate element mesh
```

```
[Ex,Ey]=coordxtr(Edof,Coord,Dof,nen); % Generate Element coordinates
```

Plot see in Figure 7.6, the mesh using *eldraw* function.

```
figure;
eldraw2(Ex,Ey,[1 4 1],Edof(:,1)); % Draw the element meshg with element numbering
figure;
eldraw2(Ex,Ey,[1 4 0]);
text(Coord(:,1),Coord(:,2),num2str(Dof(:))); % Draw the element meshg with node numbering
```

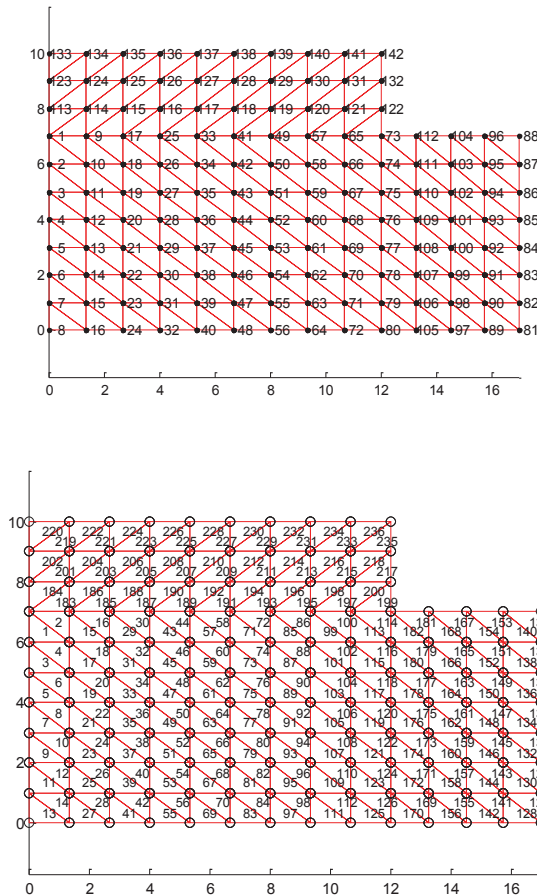


Figure 7.6. Mesh configuration of cross-section showing node numbers (left) and element numbers (right).



School of Engineering, Department of Mechanical Engineering
Blekinge Institute of Technology
SE-371 79 Karlskrona, SWEDEN

Telephone: +46 455-38 50 00
E-mail: info@bth.se